Biophysical Journal
Article

Biophysical Society

Cholesterol Increases the Openness of SNARE-Mediated Flickering Fusion Pores

Benjamin S. Stratton,[1] Jason M. Warner,[1] Zhenyong Wu,[2,3] Joerg Nikolaus,[2,3] George Wei,[1] Emma Wagnon,[1] David Baddeley,[3,4] Erdem Karatekin,[2,3,5,6,*] and Ben O'Shaughnessy[1,*]

[1]Department of Chemical Engineering, Columbia University, New York, New York; [2]Department of Cellular and Molecular Physiology, Yale University, School of Medicine, New Haven, Connecticut; [3]Nanobiology Institute, Yale University, West Haven, Connecticut; [4]Department of Cell Biology and [5]Department of Molecular Biophysics and Biochemistry, Yale University, New Haven, Connecticut; and [6]Laboratoire de Neurophotonique, Université Paris Descartes, Centre National de la Recherche Scientifique (CNRS) UMR8250, Paris, France

ABSTRACT Flickering of fusion pores during exocytotic release of hormones and neurotransmitters is well documented, but without assays that use biochemically defined components and measure single-pore dynamics, the mechanisms remain poorly understood. We used total internal reflection fluorescence microscopy to quantify fusion-pore dynamics in vitro and to separate the roles of soluble *N*-ethylmaleimide-sensitive factor attachment protein receptor (SNARE) proteins and lipid bilayer properties. When small unilamellar vesicles bearing neuronal v-SNAREs fused with planar bilayers reconstituted with cognate t-SNARES, lipid and soluble cargo transfer rates were severely reduced, suggesting that pores flickered. From the lipid release times we computed pore openness, the fraction of time the pore is open, which increased dramatically with cholesterol. For most lipid compositions tested, SNARE-mediated and nonspecifically nucleated pores had similar openness, suggesting that pore flickering was controlled by lipid bilayer properties. However, with physiological cholesterol levels, SNAREs substantially increased the fraction of fully open pores and fusion was so accelerated that there was insufficient time to recruit t-SNAREs to the fusion site, consistent with t-SNAREs being preclustered by cholesterol into functional docking and fusion platforms. Our results suggest that cholesterol opens pores directly by reducing the fusion-pore bending energy, and indirectly by concentrating several SNAREs into individual fusion events.

INTRODUCTION

A critical step in processes such as neurotransmitter or hormone release via exocytosis, intracellular trafficking, and enveloped virus infection is the creation of a fusion pore that connects membrane-enclosed compartments and allows the contents to be released (1). Most intracellular membrane fusion events, as well as exocytosis, are driven by soluble *N*-ethylmaleimide-sensitive factor attachment protein receptor (SNARE) proteins when vesicle-associated SNAREs (v-SNAREs) form complexes with target-membrane-associated SNAREs (t-SNAREs) (2). Exocytotic fusion pores are highly dynamic and may flicker repeatedly between the open and closed states before either permanently closing or dilating (3–11) (Fig. 1).

The dynamics of the pore are physiologically regulated and determine the amount, the size, and the kinetics of cargo release, with important consequences for downstream events. In chromaffin cells, basal stimulation selectively releases only small cargo through flickering fusion pores, whereas increased stimulation leads to release of all cargo sizes through pores that rapidly dilate (12). Although more challenging to detect, pore flickering also occurs during synaptic vesicle exocytosis (4,13,14) and may serve to regulate synaptic strength (15) and/or the kinetics and spatial extent of receptor activation (4).

Fusion-pore dynamics are altered by mutations in SNAREs and other components of the fusion machinery (5,8,16). Cholesterol, a major constituent of eukaryotic plasma membranes (40% (17)), synaptic vesicles (~40% (18)), and secretory granules (25% (19)), is also a key modulator of fusion-pore dynamics and rates of fusion. Pharmacological reduction of cholesterol lowered rates of exocytosis in hippocampal neurons (20) but shortened the duration of the prespike foot (PSF) in chromaffin cells, suggesting a faster transition to a fully developed pore (21). The

Submitted December 12, 2014, and accepted for publication February 4, 2016.

*Correspondence: erdem.karatekin@yale.edu or bo8@columbia.edu

Jason M. Warner, Zhenyong Wu, and Joerg Nikolaus contributed equally to this work.

Editor: Axel Brunger.

http://dx.doi.org/10.1016/j.bpj.2016.02.019

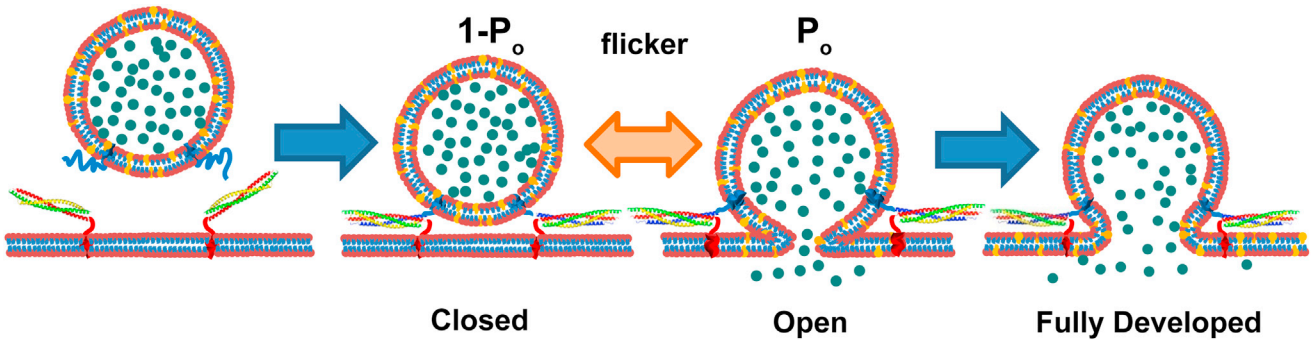

FIGURE 1 Schematic of the flickering dynamics of membrane fusion pores. A vesicle docks onto a planar membrane by complexation of vesicle v-SNAREs (*blue* on vesicle) with t-SNAREs (*red*, *yellow*, and *green* on SBL). Fusion of the membranes creates an open pore through which contents are released. Live-cell electrophysiological studies show that fusion pores may flicker rapidly and repeatedly between closed and open states, then dilate to become fully developed pores or permanently close. In this study, we track flickering of fusion pores by monitoring release of labeled vesicle membrane lipids (*yellow*) into the planar membrane (Fig. 2). Simultaneous observations of lipid and content release are also made (Fig. 3). Release is retarded because the pore is open only a fraction, P_o, of the time. To see this figure in color, go online.

presence of oleic acid, with an inverted cone geometry similar to that of cholesterol, reduced the PSF duration in PC12 and chromaffin cells (22). Introduction of ~40% cholesterol to liposome membranes increased the initial rates of fusion in a bulk liposome assay (23). In cell-cell fusion mediated by the influenza fusion protein hemagglutinin, cholesterol accelerated and increased the incidence of fusion (24).

Flickering dynamics of fusion pores are most directly measured using electrophysiological and electrochemical approaches. In amperometric traces of content release, pore flickering causes fluctuations in the low-amplitude PSF and in "stand-alone feet" that signal transient events involving partial content release without full pore enlargement (3–7). Flickering is also manifested by fluctuations in pore conductance (7,9) and membrane capacitance (11,14). From such studies, fusion pores that flicker typically do so ~2–10 times at frequencies from 40 Hz in beige mast cells to 170 Hz in chromaffin cells to 4000 Hz in ventral midbrain neurons (3,4,7). A pore height of ~15 nm, similar to that of a gap junction, is commonly assumed, in which case measured conductances imply pore radii of ~0.5–5 nm (9,11,13,14).

In small vesicles, pores were measured to flicker between two discrete states, the closed state and an open state of fixed size that varies little within or between flickering episodes. In ~25-nm-radius synaptic vesicles and microvesicles, conductance of fusion pores revealed ~10- to 20-Hz flickering between discrete open and closed states, with sharp transitions between the two and an almost constant conductance in the open state from one open event to another (13,14). In amperometric measurements of fusion pores in ~25 nm synaptic vesicles during exocytosis in ventral midbrain neurons, the initial peak value in flickering sequences was consistent between events, suggesting a fixed fully open pore state (4). In larger, ~100 nm dense-core vesicles in chromaffin cells, before dilation, flickering pores in the fully open state had approximately constant conductance from flicker to flicker, whereas pores in $\gtrsim$ 1-μm-sized large granules in beige mast cells show much more variable conductance in time during flickering (7,25,26).

A quantitative characteristic of a two-state flickering pore is its openness, P_o, the fraction of time the pore is in the open state. The analogous concept is used in the study of ion channels (27). The openness is closely related to the thermodynamic driving force for fusion, ΔF_{pore}, the free-energy difference between the open and closed states (Fig. 1). Using Boltzmann's distribution, $P_o = e^{-\Delta F_{pore}/k_BT}/(1+e^{-\Delta F_{pore}/k_BT})$, where T is temperature and k_B is Boltzmann's constant. ΔF_{pore} presumably sums downhill contributions from SNAREs and other components that drive the pore to open and uphill contributions from the lipid membranes that must bend to make the fusion pore (28). In a natural generalization to a flickering pore whose size fluctuates through a continuum of sizes, P_o is the time-averaged conductance relative to the conductance when fully open. Electrophysiological measurements suggest that P_o ~ 0.3–0.8, i.e., small free-energy differences, ΔF_{pore}, of order kT (3,4,7,10,13,14).

The mechanism that governs pore flickering is unknown, in part because methods to measure individual pore dynamics in reconstituted, biochemically defined systems have not been available. Here, we developed such a method, using total internal reflection fluorescence (TIRF) microscopy to measure flickering pores during reconstituted SNARE-mediated fusion of small unilamellar vesicles (SUVs; comparable in size to synaptic vesicles) with supported bilayers (SBLs). Due to the evanescent wave excitation with a polarized laser beam (29), individual fusion events are signaled by a rapid increase in intensity as fluorescently labeled lipids diffuse from the vesicle membrane into the SBL membrane. Consistent with rapid ($\gtrsim$ 100 Hz) pore flickering, lipids were released from the vesicle ~10-fold, and in some cases up to 100-fold, more

slowly compared to release via a continuously open pore (Fig. S1 in the Supporting Material). In experiments where we simultaneously monitored both lipid and soluble cargo release through the fusion pore, content release occurred with similar or slower kinetics compared to lipid release, also consistent with a rapidly flickering pore. Most fusion pores reseal after releasing only part of their contents. Events compatible with hemifusion (where proximal leaflets fuse, but not distal leaflets) were extremely rare. Overall, the retardation of lipid release we observe is very likely due to pore-flickering dynamics, rather than to diffusional barriers due to high curvature effects or the presence of proteins that may line the fusion pore.

From the lipid release time, we calculated the pore openness, P_o (Fig. 1), and vesicle size for each event. For most lipid compositions, lipid bilayers controlled pore flickering: SNAREs had little effect, and cholesterol increased pore openness, consistent with its ability to lower fusion-pore membrane bending energy. With higher, physiological cholesterol levels in target membranes, the presence of SNAREs dramatically opened flickering pores. Thus, in addition to its direct role, cholesterol synergistically facilitates pore opening by SNARE proteins. Our results suggest that this effect derives from cholesterol-mediated clustering of t-SNAREs at the fusion site.

MATERIALS AND METHODS

Materials

1-palmitoyl-2-oleoyl-*sn*-glycero-3-phosphocholine (POPC), 1,2-dioleoyl-*sn*-glycero-3-phosphocholine (DOPC), 1-stearoyl-2-arachidonoyl-*sn*-glycero-3-phosphoethanolamine (SAPE), 1,2-dioleoyl-*sn*-glycero-3-phospho-(1′-myo-inositol-4′,5′-bisphosphate) (PI(4,5)P2), 1,2-dioleoyl-*sn*-glycero-3-phosphoethanolamine-N-(lissamine rhodamine B sulfonyl) (LR-PE), 1,2-dioleoyl-*sn*-glycero-3-phosphoethanolamine-N-(7-nitro-2-1,3-benzoxadiazol-4-yl) (NBD-PE), 1,2-dioleoyl-*sn*-glycero-3-phosphoethanolamine-N-[methoxy(polyethylene glycol)-2000], and cholesterol were purchased from Avanti Polar Lipids (Alabasater, AL). PI(4,5)P2, only found in plasma membranes (30), and NBD-PE, used to check SBL fluidity using fluorescence recovery after photobleaching (31), were included only in the t-SNARE SBLs. In some experiments, instead of LR-PE, we used the lipid probes 1,1′-dioctadecyl-3,3,3′,3′-tetramethylindocarbocyanine perchlorate (DiI, or DiIC18 (3); D-282, Invitrogen, Carlsbad, CA) or 1,1′-dioctadecyl-3,3,3′,3′-tetramethylindodicarbocyanine perchlorate (DiD, or DiIC18 (5); D-307, Invitrogen). The soluble content marker sulforhodamine B (SRB; S-1307, Invitrogen) was purchased from Invitrogen.

Recombinant protein expression and purification

Recombinant VAMP2, syntaxin-1, and SNAP25 were expressed, purified, and reconstituted into SUVs, as described in detail previously (31,32). We used lipid/protein ratios of 200 and 20,000 for the v-SUVs and t-SBLs, respectively. Even for the smallest v-SUVs (R_{ves} = 10–20 nm), this provides enough copy numbers (5–17) of externally facing v-SNAREs per SUV, because efficient fusion in this assay requires $\gtrsim$5 SNARE complexes (32). Thus, our results for the number of t-SNAREs recruited for fusion (see Fig. 5 *A*) are not limited by the number of v-SNAREs present on vesicles.

Preparation of SUVs and SBLs

For experiments monitoring lipid mixing alone, we used the method of (31,32), but with different lipid compositions, as in Table 1 (SUV and SBL compositions are listed separately in Tables S1 and S2). We included either 0.8 mol % LR-PE or 1 mol % DiI as lipid markers, except in the case of α^{+}_{chol}, where 0.62 mol % LR-PE was used (Table S1).

For simultaneous monitoring of both lipid and content release, we included 1 mol % DiD as the lipid marker and encapsulated the soluble content marker SRB into v-SUVs. To do so, we followed the protocol of Kyoung et al. (33), with the following modifications. Dilution of the lipid, protein, and detergent mixture was followed by dialysis against 4 L of buffer overnight at room temperature. v-SUVs were then passed through a CL-4B column (Sepharose CL-4B, 17-0150-01, GE Healthcare, Little Chalfont, United Kingdom) to remove free SRB. SRB concentration was 10 or 50 mM. The lipid/protein ratio for v-SUVs was 200, as in single-color lipid-mixing experiments. We used the following lipid compositions for the v-SUVs: 67:12:15:5:1 POPC/DOPS/SAPE/PEG2KPE/DiD or 23.55:12:15:45:3.45:1 POPC/DOPS/SAPE/Ch/PEG2KPE/DiD. The t-SBLs contained one t-SNARE complex for every 20,000 lipids and were composed of 64.5:12:15:3:5:0.5 POPC/DOPS/SAPE/PIP2/PEG2KPE/NBD-PE.

Microfluidic flow channels and microscopy

Fabrication of microfluidic flow channels, formation and characterization of t-SNARE-reconstituted SBLs in the channels, and detection of fusion events are described in detail in Karatekin and Rothman (31). In this assay, fusion of single v-SNARE reconstituted liposomes (v-SUVs) with t-SNARE-bearing SBLs is observed at frame rates of 32/s (full frame) to 60/s (from a cropped region of interest). These correspond to frame durations of 31 and 17 ms, respectively. Frame durations <~15 ms resulted in lower signal/noise ratios that made tracking of single LR-PE fluorescently labeled lipids difficult. One pixel corresponded to 267 nm in the sample plane. LR-PE or DiI fluorescence was excited using an s-polarized (perpendicular to the plane of incidence) 532 nm laser beam.

To determine the areal lipid density in the membranes, $\rho_{lip} = 1/(f_{lip}\, a_{lip})$, where f_{lip} is the fraction of lipids that are labeled, we assumed a lipid headgroup area of $a_{lip} = 0.8$ nm^2 for PC/PS/PE/PIP2 and PC/PS compositions and $a_{lip} = 0.6$ nm^2 for PC/PS/PE/PIP2/Ch+ and PC/PS/PE/PIP2/Ch compositions (34).

Some of the data were obtained using an inverted microscope (IX81, Olympus, Center Valley, PA) equipped with an EM-CCD camera (iXon Ultra, Andor, Belfast, United Kingdom) and the Olympus CellTIRF TIRF microscopy (TIRFM) accessory. The microscope and data acquisition were controlled by Micro-Manager (University of California San Francisco). A 100×/1.49 NA oil TIRF objective (UAPO N, Olympus) was used. All experiments were carried at 32°C (Thermo Plate TOKAI HIT, Olympus). Images were collected with a frame duration of 17 ms (full frame). We used a 488 nm laser for FRAP measurements and a 561 nm laser for detecting LR-PE or DiI during fusion.

TABLE 1 Lipid Compositions Used in This Study

	Ch (%)	PC (%)	PS (%)	PE (%)	PIP2 (%)
POPC/DOPS/SAPE/PIP2	–	60/64	14/14	18/18	4/0
POPC/DOPS/SAPE/PIP2/Ch	10/45	55/24	12/12	15/15	3/0
POPC/DOPS/SAPE/PIP2/Ch+	45/45	19/23	12/12	15/15	3.9/0
DOPC/DOPS	–	80/79	15/15	–	–

Each entry shows the two mole fractions in the SBL membrane/vesicle membrane. In addition, each composition contained 3.45–5.0 mol % PEG2KPE, and 0.6–1.0 mol % lipid marker (LR-PE, DiI, or DiD, the latter only for content-release experiments). See Materials and Methods and Tables S1 and S2 for details.

To estimate the evanescent field penetration depth, we measured the angle of incidence, θ, of the excitation beam with respect to the normal to the imaging plane, and used the expression $\delta_{TIRF} = \lambda_o/4\pi\,(n_g^2 \sin^2\theta - n_w^2)^{-1/2}$ (29), where $\lambda_o = 532$ nm is the laser wavelength, and $n_g = 1.52$ and $n_w = 1.33$ are the refractive indices of glass and water, respectively. For this, we coupled a 2 cm × 2 cm × 2 cm BK7 glass cube (Thorlabs, Newton, NJ) to the TIRF objective using oil that matched the refractive index of glass. At angle θ, used to generate TIR in the fusion experiments, the beam went undeflected into the cube and emerged from one side refracted at the glass-air interface and projected onto a wall. Simple geometry based on the beam position on the wall and the position of the objective, along with the known refraction at the cube-air interface, allowed calculation of the incidence angle, $\theta = 73.5$–$77.4°$ ($\delta_{TIRF} = 65$–71 nm), with the highest intensity spot at 75°, corresponding to $\delta_{TIRF} = 68$ nm. This value is used in the subsection The size of a docked vesicle can be directly inferred from the docked vesicle intensity in TIRFM (and see Fig. 6 *D*).

Single lipid-label measurements

We tracked single lipids using ImageJ and Speckle TrackerJ, the tracking plugin described in (35). For details, see Fig. S2, *A–C*.

Analysis of single-vesicle events

We identified fusing vesicles by eye and tracked them using the ImageJ plugin Speckle TrackerJ (35). We used fusing vesicle trajectories to train Speckle TrackerJ to track the remaining vesicles that dock. For each fusion event, the total intensity in a region of interest was computed with Matlab from the trajectories obtained from SpeckleTrackerJ.

Curve fitting

We performed all curve fitting using the Curve Fitting Toolbox in Matlab with linear or nonlinear least-squares optimization.

Simultaneous detection of lipid and content release

For these experiments, we used an Olympus IX81 microscope, custom-modified for polarized TIRF excitation and two-color detection. SRB and DiD fluorescence was excited using 561 nm (04-01 series, Cobolt Jive, Solna, Sweden) or 638 nm (LuxX, Omicron Laserage, Rodgau-Dudenhofen, Germany) lasers, respectively, through an Olympus PlanApo 60×/1.45 Oil TIRF objective, using *s*-polarized light. We split the emission using a 640 nm dichroic mirror (ZT640rdc-UF2, Chroma, Bellows Falls, VT), and projected the two beams that went through a short (570–620 nm; ET595/50m EM, Chroma) and a long (662.5–737.5 nm; ET700/75m EM, Chroma) wavelength emission filter side-by-side on the same electron-multiplying charge-coupled device (Ixon Ultra, Andor). One pixel corresponded to 265 nm. Exposure time was 17.8 ms (duty cycle, 18.3 ms). We recorded 3,300 frames (60 s) for a total of 26 movies. Image stacks were analyzed using ImageJ and home-made Python scripts.

RESULTS

Single-event TIRF-based fusion assay

We used a recently established TIRFM-based fusion assay (31,35) to monitor fusion of individual, neuronal v-SNARE-containing SUVs with neuronal t-SNARE-reconstituted planar bilayers supported on a soft poly(ethylene glycol) (PEG) cushion in microfluidic flow channels, with 0.8 mol % LR-PE or 1 mol % DiI as fluorescent lipid markers (Fig. 2 *A*).

Four membrane lipid compositions were tested (Table 1): a model DOPC/DOPS mixture (31,32,36) and three compositions that included PI(4,5)P2 in SBL membranes and SAPE and varying amounts of cholesterol, 0%, 10%/45%, and 45%/45%, in the SBL/SUV membranes (POPC/DOPS/SAPE/PIP2, DOPC/DOPS/SAPE/PIP2/Ch, POPC/DOPS/SAPE/PIP2/Ch+, see Table 1 and Materials and Methods). All lipid compositions used in this study are expected to form fluid bilayers, as the transition temperature of each component is <0°C. Accordingly, we saw no evidence of phase separation, either using fluorescent probes or when we tracked single lipid labels. PE is found at levels up to 15% in synaptic vesicles, secretory granules, and plasma membranes (18), has negative spontaneous curvature, and promotes fusion in model systems (37). The signaling lipid PI(4,5)P2 is present in small amounts in the inner leaflet of

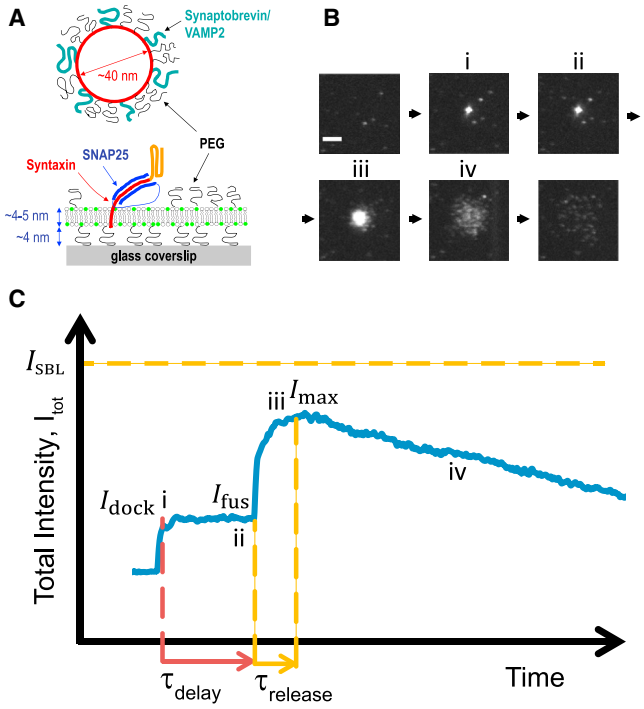

FIGURE 2 Using TIRFM to measure lipid mixing and fusion-pore flickering dynamics. (*A*) Vesicles reconstituted with v-SNAREs (synaptobrevin/VAMP2) fuse with a target SBL reconstituted with cognate t-SNAREs (syntaxin and SNAP25). Membranes are PEGylated to prevent nonspecific interactions, and 0.6–1% of lipids are fluorescently labeled. (*B*) TIRF sequence during a typical fusion event, viewed from beneath the coverslip in (*A*). When the vesicle docks onto the SBL, a spot appears (*i*). At a later time, τ_{delay}, fusion occurs (*ii*) and the spot brightens as labeled lipids diffuse into the SBL (*ii*→*iii*). Individual lipids are discernible by stage iv. The box size is 22 μm × 22 μm, 82 × 82 pixels, and the scale bar represents 5 μm. (*C*) Typical time course of total fluorescence intensity, I_{tot}, integrated over the box in (*B*), from which we extracted the lipid release time, $\tau_{release}$. After lipid release into the SBL, I_{tot} would increase to the value I_{SBL} were it not for bleaching (*iii*→*iv*) ($I_{max} < I_{SBL}$). To see this figure in color, go online.

the plasma membrane (1–2%) (30) and interactions with the t-SNARE syntaxin concentrate PIP2 at docking and fusion sites (38). Cholesterol plays a facilitating role in biological and model fusion reactions that is well-documented (20,23,24), including its modulation of the fusion pore (21).

Lipid compositions used in this study

For most experiments, we recorded movies of docking and fusion events, monitoring only lipid markers. For each fusion event, we measured the total intensity versus time, $I_{tot}(t)$, summed over all pixels in a box drawn around the fusing vesicle (Fig. 2, *B* and *C*). After docking of a vesicle to the SBL, when the intensity increases to a value I_{dock}, after a delay time, τ_{delay}, fusion is announced by a rapidly increasing intensity (39) as labeled lipids, initially in the vesicle membrane, begin to be released into the SBL through the bilayer walls of the fusion pore (Fig. 1). The intensity of labeled lipids in the vesicle, LR-PE or DiI, is reduced by a certain average factor, λ_{TIRF}, because the evanescent excitation field, with a decay length of ~68 nm (Materials and Methods), decays with distance from the SBL, and its polarization is a worse match for the dipole orientations of the fluorescent lipid labels when they reside in the spherical vesicle (29). The delay time distributions revealed a fast-fusing SNARE-mediated population and a slowly fusing, nonspecific population (32) (Fig. S2, *E* and *F* and Supporting Material).

Lipid and content release are retarded by flickering fusion pores

We used the fluorescence increase that accompanies diffusion of a labeled vesicle lipid into the SBL to track the release process and hence infer properties of the fusion pore. The fluorescence increases by the inverse of the mean intensity reduction factor for lipids in the vesicle, λ_{TIRF}. As the increase is instantaneous upon lipid transfer, we could measure the fraction of lipids transferred with high sensitivity and with temporal resolution limited only by acquisition frame rates (up to ~100 Hz), not by the time required for the lipids to diffuse a distance larger than the optical resolution (~250 nm) to detect their spread. Individual lipid labels became discernible as they diffused away from the fusion site, eventually disappearing in single bleaching steps (35). The release of lipids into the SBL occurred over a timescale, $\tau_{release}$, when the intensity increased toward a plateau but then decreased due to bleaching (Fig. 2 *C*).

Intriguingly, lipid release times were far greater (~30–250 ms; Fig. S1) than expected for a permanently open pore (~10 ms, the lipid diffusion time on the scale of a typical vesicle (40)). This suggested that fusion pores were flickering and spending only a fraction of the time in the open state, i.e., the pore openness, P_0, was significantly less than unity.

To test this possibility, we studied fusion events while simultaneously monitoring lipid and content release. We encapsulated 10 or 50 mM soluble content label SRB into v-SUVs that also contained 1 mol % DiD as the lipid marker. We excited both markers simultaneously using 561 nm (for SRB) and 638 nm (for DiD) lasers. We split the emission into two beams that went through short (570–620 nm) and long (662.5–737.5 nm) wavelength filters for the SRB and DiD emissions, respectively, and projected the two emission signals side by side onto an EMCCD chip. Movies were recorded with 18.3 ms time resolution for 60 s. SRB was encapsulated into vesicles at highly self-quenched concentrations. Consequently, for most docked vesicles, initially only the DiD lipid signal was visible. However, within a frame after the lipid signal began to increase due to transfer of lipids into the SBL, the content signal also began to increase due to dequenching effects caused by dilution of the content labels as molecules escaped through the fusion pore (Fig. 3). For >80% of all events for which simultaneous lipid and content release could be observed (74 of 91 events), the initial pore resealed after releasing all of the lipid labels but only a fraction of the content labels. More than 20% of these partial-content-release events were followed seconds later by a sudden decrease in content signals (Fig. S7). We presumed this was either because the pore reopened with sufficient width to allow rapid release of contents, or because the vesicle burst due to accumulated photodamage (41). Whatever its origin, the late disappearance of content signal showed that the initial increase in content signal was not due to content markers being released and then trapped in the space between the SBL and the substrate, as found in a previous study using SBLs directly supported on a quartz substrate, without a soft spacer such as the PEG layer used here (41).

Content- and lipid-release kinetics either occurred at comparable rates within a few frames (24/91 events), or content release was visibly slower (46/91 events; see Fig. 3 for an example). For the remaining events, we could not reliably compare the kinetics.

Signal changes compatible with hemifusion (lipid mixing preceding content mixing) were observed very rarely (2 of 91 events). Hemifusion could also be detected in single-color experiments monitoring lipid labels alone, as it would leave about half the initial docked-vesicle lipid intensity intact after dispersion of the outer-leaflet lipid markers into the SBL (31,32). Monitoring lipid signals alone, we found that such events were very rare, consistent with our previous studies (31,32).

In summary, simultaneous monitoring of lipid and content release showed that the two processes commenced within a single frame of one another (18.3 ms), and the kinetics of both content and lipid release were much slower than expected for permanently open pores $\gtrsim$ 2 nm in

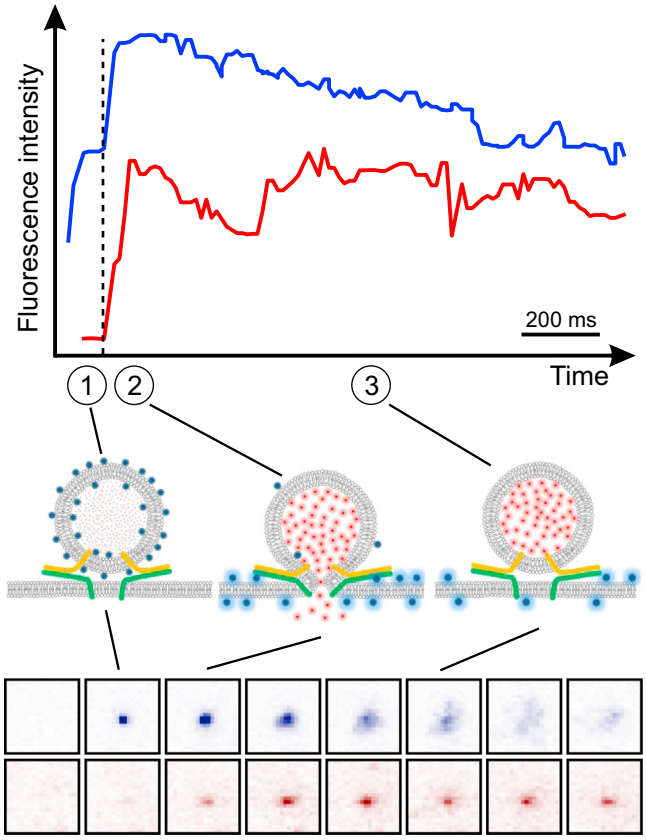

FIGURE 3 Simultaneous content and lipid release using TIRFM. v-SUVs contained 1 mol % DiD lipid dye and encapsulated 10 or 50 mM soluble content marker SRB. DiD and SRB were excited simultaneously using 638 nm and 561 nm laser lines, respectively. The emission was split and filtered to observe DiD (*top*, *blue trace*) and SRB (*lower*, *red trace*) fluorescence signals simultaneously projected onto an EMCCD detector. Total intensities from a region 20 pixels × 20 pixels (5.3 μm × 5.3 μm) is plotted for both the lipid (*upper*, *blue trace*) and content (*lower*, *red trace*) signals for a representative event. Snapshots from the lipid (*top sequence*, *blue*) and content (*bottom sequence*, *red*) signals are shown in inverted false color. When docking was clearly visible in the lipid channel, the content channel was still dim, because SRB was encapsulated at self-quenching concentrations (*1*). In the same frame where the lipid signals start to increase, announcing lipid mixing, the content signals also increase (*dashed vertical line*) due to dilution and dequenching of encapsulated SRB as some molecules escape through the pore. Once lipid transfer is complete (shortly after the maximum in the *upper blue trace*), the intensity in the lipid channel decreases due to photobleaching, as in Fig. 2. The SRB signals remain stable after lipid release (but bleach slowly (*3*)), indicating that the pore resealed after partial release of contents. In this example, initial lipid and content release occurred with comparable kinetics (*2*) within a few frames (each 18.3 ms apart). In other cases, release was markedly slower (see Fig. S7). To see this figure in color, go online.

diameter. These findings strongly suggest that the fusion pores we observe flicker, and the effect is to retard both lipid and content mixing. We note that during fusion reactions mediated by the influenza fusion protein hemagglutinin, electrophysiologically detected fusion pore opening preceded detectable lipid and content release by seconds (42). Zimmerberg et al. (42) argued that this was caused by an early transition to a larger pore rather than by retardation due to the effect of fusion proteins, as previously proposed (43). Our results suggest that the size and flickering dynamics of the pore itself set lipid and content release rates, since the onset of both was simultaneous. Moreover, retardation of lipid diffusion was the same for specific and nonspecific fusion, suggesting that the retardation is not caused by the SNARE proteins (Fig. 4 *C*).

For the remainder of the study, we used lipid release kinetics to characterize the flickering statistics of fusion pores, as the signal/noise ratio in single-color measurements of lipid release allowed tracking of single lipid labels and calculation of vesicle size for individual events. This was needed to compute the pore openness, as detailed below. Unless specified otherwise, all experimental results presented below are from single-color lipid-marker measurements.

Fusion pore openness, P_0, is quantitatively related to the lipid release time, $\tau_{release}$

We established a relationship that enabled us to deduce the pore openness, P_o, from the time for lipids to be released from the vesicle into the SBL, $\tau_{release}$, that we measured for each fusion event from the TIRFM intensity curve (Fig. 2 *C*). A mathematical model of lipid release through a flickering pore showed that

$$P_o = \frac{A_{ves} b}{2\pi r_p D_{lip} \tau_{release}} \quad (1)$$

(see Supporting Material). For a two-state (open/closed) pore, P_o is the fraction of the time in the open state, but Eq. 1 is equally valid for a flickering pore with a size varying continuously in time, when P_o is the time-averaged pore radius relative to the fully open radius. In Eq. 1, A_{ves} is the vesicle area and D_{lip} the lipid diffusivity, which we measured directly (see below). This equation states that $P_o = g\,\tau_{ves}/\tau_{release}$, where $\tau_{ves} = A_{ves}/D_{lip}$, the time for a lipid to diffuse a distance of the order of the vesicle size, would be the diffusion-controlled release time for a fully open pore (to within logarithmic corrections). For an infrequently open pore, $P_o < 1$, the release time, $\tau_{release}$, is much greater than τ_{ves}. P_o is the ratio of these two timescales times a factor $g = b/2\pi r_p$ reflecting the role of pore geometry on lipid release rate.

We took a pore height of $b = 15$ nm, as is commonly assumed, and the radius of the fully open conducting pore was taken to be 1 nm, as reported for smaller vesicles (4,9,11,13,14). This implies a value of $r_p = 3$ nm as the fully open pore radius in Eq. 1 is the effective value seen by a diffusing lipid and so includes half the bilayer thickness, taken to be 2 nm (Fig. S1 *A*). Equation 1 states that a flickering pore more often in the closed state (lower P_o) releases lipids more slowly (larger $\tau_{release}$).

For a given fusion event, the vesicle area, A_{ves}, in Eq. 1 is unknown, as sizes varied significantly. The docked

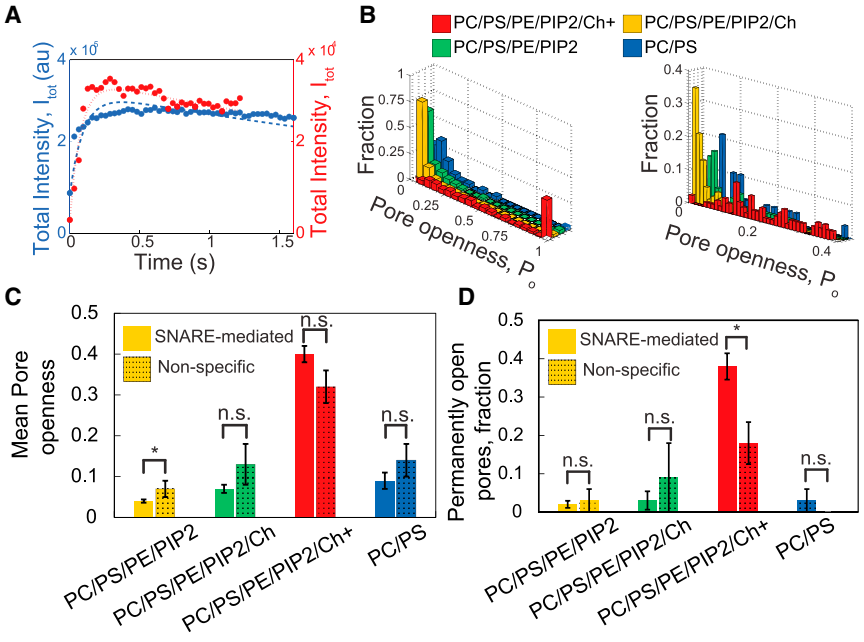

FIGURE 4 Openness statistics of SNARE-mediated flickering fusion pores. (*A*) TIRF intensity versus time after fusion for two typical SNARE-mediated fusion events. The time course of the red trace (*short-dashed curve fit*, PC/PS) is well fit by Eq. 3 for a flickering pore, with openness $P_o = 0.09$ (*short-dashed curve*). The fit from Eq. 3 is poor for the blue trace (*long-dashed curve fit*, PC/PS/PE/PIP2/Ch+, 45% cholesterol), with nominal $P_o = 3.48$ (*long-dashed curve*), flagging a permanently open pore (Eq. 4). (*B*) SNARE-mediated fusion pores flicker and are dramatically opened by increasing cholesterol content. (*Left*) Flickering-pore openness, P_o, and the fraction of pores that are permanently open ($P_o = 1$ column) for each of the four lipid compositions studied (Table 1). The bin size is 0.05. (*Right*) Blowup of $P_o \leq 0.4$ data (bin size, 0.01). (*C* and *D*) SNAREs play little or no role in fusion-pore flickering unless cholesterol content is high. Mean pore openness (*C*) and fraction of pores that are permanently open (*D*) versus composition for SNARE-mediated and SNARE-independent fusion-pore dynamics. Error bars in (*C*) and (*D*) indicate the mean ± SE; $^*p < 0.05$ using Student's *t*-test. To see this figure in color, go online.

vesicle intensity, I_{dock} (Fig. 2 *C*) is the best measure of vesicle size, being the earliest and least affected by bleaching. The difficulty is that the relation between A_{ves} and I_{dock} is not a priori known, since the intensity of fluorescently labeled lipids in the vesicle is unknown. However, we directly measured I_{lip}, the single lipid intensity for lipids in the planar SBL (see below). Thus, we used the TIRFM curve for each event to determine the fluorescence intensity reduction factor, λ_{TIRF}, namely the ratio of total intensities before and after lipid release. The area is then

$$A_{ves} = I_{dock} / \left(\lambda_{TIRF} I_{lip} 2\rho_{lip}\right). \quad (2)$$

Here, ρ_{lip} is the areal density of fluorophores in each leaflet of the vesicle membrane and $\lambda_{TIRF}\, I_{lip}$ is the single labeled lipid intensity for a lipid in the vesicle, averaged over all locations in the vesicle membranes, including the reduction factor, λ_{TIRF}, relative to the value I_{lip} in the SBL. The reduction factor depends on vesicle size in a complex fashion (see below).

In practice, direct extraction of $\tau_{release}$ and λ_{TIRF} from the measured fluorescence signal, $I_{tot}(t)$, is difficult due to bleaching of labeled lipids in the SBL, with bleaching time, τ_{bleach}, of ~3.5 s for LR-PE (Figs. 2 *C* and S2 *C*). Thus, we used the expression predicted by our model for the TIRFM signal, given by

$$\frac{I_{tot}(t)}{I_{fus}} = e^{-t/\tau_{release}} + \frac{\left(e^{-t/\tau_{bleach}} - e^{-t/\tau_{release}}\right)}{\lambda_{TIRF}\left(1 - \tau_{release}/\tau_{bleach}\right)} \quad (3)$$

(see the Supporting Material). We neglect the slower bleaching in the vesicle (τ_{bleach} ~ 18 s; Fig. S2 *D*). Our procedure was to fit the predicted expression (Eq. 3) to the experimentally measured signal and determine the two crucial parameters $\tau_{release}$ and λ_{TIRF} as best-fit parameters. A related situation was mathematically modeled in (44), in which labeled lipids diffused through a narrow pore during cell-cell fusion and the effects of fluorescence dequenching were calculated.

Permanently open pore

In the above, lipid release is limited by flickering, and the fraction of labeled lipids remaining in the vesicle a time *t* after the instant of fusion (when the pore first opens) decays exponentially, $\phi_{ves} = e^{-t/\tau_{release}}$ (Eq. S8). We will see that our experiments show that a fraction of pores do not flicker, but are permanently open. In this case, release is limited by diffusion, and our model shows that the decay has a qualitatively different inverse time dependence and the TIRFM intensity time course is different:

$$\frac{I_{tot}(t)}{I_{fus}} = e^{-t/\tau_{bleach}}\left[\phi_{ves}(t) + \left(\frac{1 - \phi_{ves}(t)}{\lambda_{TIRF}}\right)\right], \quad (4)$$
$$\phi_{ves}(t) = \tau_{ves}/t.$$

SNARE-mediated fusion pores flicker or are permanently open

We used the following procedure, which yielded the pore openness, the vesicle radius, R_{ves}, and the intensity reduction factor, λ_{TIRF}, for each fusion event. 1) We first measured the bleaching time, τ_{bleach}, the diffusivity, D_{lip}, and the intensity, I_{lip}, of single fluorescently labeled lipids in the SBL (Materials and Methods and Fig. S2). 2) For each detected

fusion event, we extracted the docked fusion intensity, I_{dock}, and the intensity at the instant of fusion, I_{fus}, from the measured fluorescence intensity curve, $I_{tot}(t)$ (Fig. 2 *C*). 3) We fit the predicted TIRF intensity curve, $I_{tot}(t)$ (Eq. 3), to the experimental curve using the fluorescence reduction factor, λ_{TIRF}, and lipid release time, $\tau_{release}$, as fitting parameters. 4) We used Eq. 2 to obtain the vesicle area and radius, and then Eq. 1 to obtain the pore openness.

Applying this procedure to the fast SNARE-mediated fusion events we found that pores flickered with pore openness of $0.01 \lesssim P_o \lesssim 0.9$, suggesting free energies of pore formation of $-2\ \mathrm{kT} \lesssim \Delta F_{pore} \lesssim 5\ \mathrm{kT}$ (Fig. S1 *B*). Although most pores flickered, in many cases, the analysis returned a nominal P_o value exceeding unity, indicating a fully open pore, $P_o = 1$. To reinforce this conclusion, we tested these pores for inverse time-release kinetics, $\phi_{ves} \sim 1/t$, the signature of a permanently open pore (Eq. 4). For this test, we used larger vesicles, $R_{ves} \geq 25$ nm, whose slower release kinetics were more accessible. The exponent of the best-fit power law to the pooled release kinetics was close to that predicted (-0.99 ± 0.22), compared to a best-fit exponent of -0.68 ± 0.09 for flickering pores with $P_o < 0.15$ (Fig. S3 *B*).

As an additional test of our assumption that slow lipid release reflects flickering pores (Eq. 3) rather than restricted lipid diffusion due to high curvature or protein crowding effects at the pore (45) we repeated experiments using a different label, replacing LR-PE with DiI. We found statistically insignificant differences in pore openness values (Supporting Material and Fig. S6), consistent with normal lipid diffusion through the pore.

We note that a "permanently" open pore is one that remained open long enough to release all labeled lipids, approximately the lipid diffusion time for the vesicle size, τ_{ves} (multiplied by a logarithmic factor of order unity involving the pore diameter (40)). Thus, such a pore could in fact be slowly flickering, with a frequency of $\lesssim 100$ Hz if we take a typical τ_{ves} ~10 ms. In fact, we found no vesicle size dependence in the fusion statistics (Supporting Material and Fig. S4), suggesting that such pores remained open for sufficiently long that even the largest vesicles studied (R_{ves} ~ 80 nm) had enough time to empty their labeled contents. For these large vesicles, this would occur in an estimated time of order τ_{ves} ~ 50 ms. This suggests that the pores we identify as open flickered at frequencies of <20 Hz.

Cholesterol promotes the open state of the fusion pore

When pore statistics were classified according to the composition of the fusing membranes, there was a strong correlation of flickering pore openness with the presence of cholesterol (Fig. 4, *B–D*). For cholesterol-free compositions, the mean flickering pore openness was $\overline{P_o} = 0.04$, although only ~2% were permanently open. With 45% (10%) cholesterol in the SUV (SBL) membranes, the mean P_o doubled, but the permanently open fraction was unchanged. For compositions better mimicking physiological conditions, which included 45 mol % cholesterol, the effect was dramatic: relative to cholesterol-free membranes, the flickering pore openness and the permanently open fraction increased ~10-fold and ~20-fold, respectively.

Our simultaneous lipid- and content-release measurements corroborated these findings. When v-SUVs and t-SBLs both lacked cholesterol, content labels were released more slowly than lipid markers in 54% of all events (43 of 79), both types of release occurred within a few frames for 22% of events (17 of 79), and the kinetics could not be reliably compared due to weak signals for 24% of events (19 of 79). In contrast, when the v-SUVs included 45 mol % cholesterol, both types of release occurred rapidly within a few frames in 58% of all events (7 of 12), whereas contents were released more slowly for only 25% of events (3 of 12). For 17% of events (2 of 12) we could not reliably compare release kinetics.

SNARE proteins have little effect on the fusion-pore openness unless physiological levels of cholesterol are present

To distinguish the respective roles of SNAREs and lipid bilayers in fusion-pore dynamics, we repeated the above analysis for the slow nonspecific fusion events, for which we assumed the fusion-pore dynamics are not SNARE mediated (32). Both without cholesterol and with 45% (10%) cholesterol in the SUV (SBL) membranes, these events showed pore openness and permanently open pore fractions that were statistically indistinguishable from SNARE-mediated events, except that there was a small increase in P_o with no cholesterol ($n = 353$ SNARE-mediated events, $m = 68$ nonspecific events, Fig. 4, *C* and *D*). This suggests that the lipid bilayers themselves governed pore dynamics with little influence from SNARE proteins.

To test this conclusion, we measured fusion between protein-free SBLs and v-SNARE-containing SUVs (Supporting Material and Fig. S2 *F*). For the same compositions, the delay times and openness were statistically indistinguishable from those for the slow component in the presence of v- and t-SNAREs. This is consistent with the hypothesis that pore dynamics for the slow component reflect the physical properties of lipid bilayers only.

A qualitatively different picture emerged at physiological cholesterol levels in all membranes (45%): SNARE proteins then increased the fraction of open pores significantly, from 18% to 38% (Fig. 4 *D*). Thus, at high concentrations cholesterol opens pores both indirectly, by activating SNARE-mediated pore opening, and directly through its influence on the lipid membranes.

With physiological amounts of cholesterol, fusion is so accelerated that there is insufficient time to recruit additional t-SNAREs to the fusion site after docking

Next, we examined the effect of cholesterol on the docking-to-fusion delay times for the fast SNARE-mediated fusion events, and we applied the model of (32), which assumes that fusion is limited by the diffusive recruitment of t-SNAREs to the fusion site once a vesicle has docked. Delays were ~2-fold greater in the presence of intermediate amounts of cholesterol (45% and 10% in the SUV and SBL membranes) and sufficient for three to six t-SNAREs to have been recruited, consistent with literature values for the number of SNAREs required for fusion (32,36) (see Fig. 5 *A* and Supporting Material).

By contrast, at physiological cholesterol levels (45% in all membranes), the delay times were ~3-fold smaller, too short for even one additional t-SNARE to have been diffusively recruited if one assumes a uniform spatial distribution of t-SNAREs. This was unexpected, since lipid diffusivity was reduced ~4-fold at these cholesterol levels (Table S3), suggesting that delay times would be greater. Thus, t-SNAREs were presumably already clustered at docking sites in sufficient numbers to trigger fusion, consistent with cholesterol-mediated t-SNARE clustering observed in cells (46–49).

Consistent with these results, the probability that a docked vesicle underwent SNARE-mediated fusion during the observation time increased ~3-fold at the highest cholesterol levels (Fig. 5 *B*).

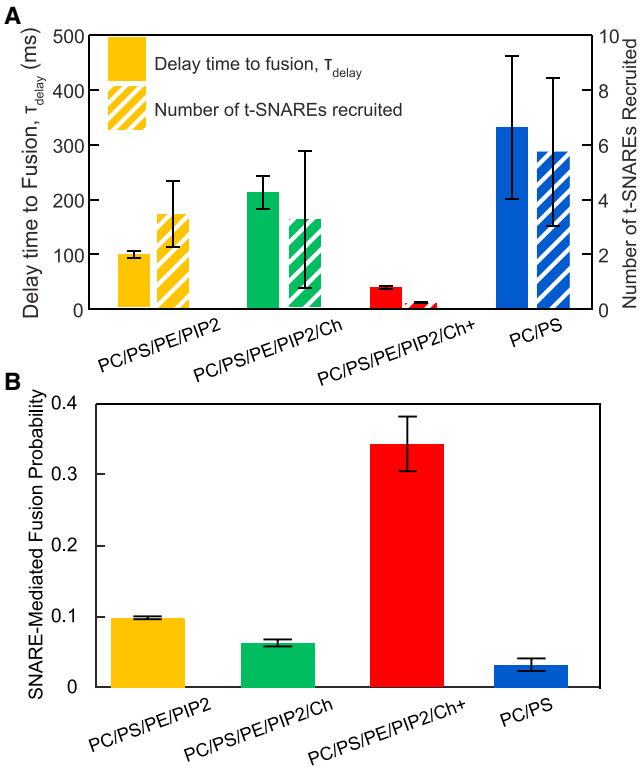

FIGURE 5 Physiological amounts of cholesterol accelerate fusion by clustering t-SNAREs. (*A*) Delay times to SNARE-mediated fusion after vesicle docking versus membrane lipid composition (*solid bars*) and calculated number of t-SNAREs assumed recruited by diffusion to the fusion site during the delay time (*striped bars*). Lower amounts of cholesterol (*yellow* (PC/PS/PE/PIP2) and *green* (PC/PS/PE/PIP2/Ch)) increase delay times, consistent with the reduced lipid diffusivities, but the number of t-SNAREs recruited for fusion is unchanged. At physiological cholesterol (PC/PS/PE/PIP2/Ch+), fusion is so accelerated that there is insufficient time to recruit any additional t-SNAREs after docking, suggesting that t-SNAREs are preclustered. (*B*) Physiological cholesterol levels increase the probability ~3-fold that a docked vesicle undergoes SNARE-mediated fusion (as opposed to nonspecific fusion or no fusion) before complete bleaching (~20 s). To see this figure in color, go online.

Fluorescence reduction factor and vesicle size are unique functions of the docked-vesicle intensity

Our procedure entailed measuring the docked-vesicle intensity, I_{dock}, for each fusion event and extracting the intensity reduction factor, λ_{TIRF}, by fitting our model to the fluorescence profile (Figs. 2 *C* and see 4 *A*). An important self-consistency check is that λ_{TIRF} is a unique function of I_{dock}, since the value of I_{dock} fixes the vesicle size and hence the value of λ_{TIRF} (Fig. 6 *A*). When we pooled the values for several compositions labeled with LE-PE and included nonspecific fusion events, the λ_{TIRF} -versus- I_{dock} data collapsed around a definite curve (Fig. 6 *B*). The R_{ves}-versus- I_{dock} data collapsed similarly (Fig. 6 *C*). Thus, our method satisfies this self-consistency check.

DISCUSSION

Single exocytotic fusion pores were first detected almost 30 years ago (50,51), shortly followed by observations of rapid flickering between the open and closed states (26,50). Neuroendocrine cells regulate hormone release by adapting the incidence and flickering dynamics of fusion pores to physiologic inputs (12). Pores also flicker during synaptic vesicle release, but the prevalence is less established, in part because of technical difficulties in probing pore properties during synaptic-vesicle exocytosis using direct electrical approaches. The few such measurements showed that 3–40% of pores flicker during synaptic-vesicle release (4,13) and that the flickering dynamics are regulated by phosphorylation (4). Possibly the most convincing data are from midbrain neurons that form "social" synapses and release dopamine that is sensed by receptors some distance (several micrometers) away from release sites (4). For such volume transmission, pore flickering would control the kinetics and spatial extent of receptor activation (4). In addition, "whispering" synapses at which downstream receptors are not activated may be associated with slow release through flickering fusion pores (15), and neurotransmitter release through transient pores may facilitate rapid recycling of synaptic vesicles (4).

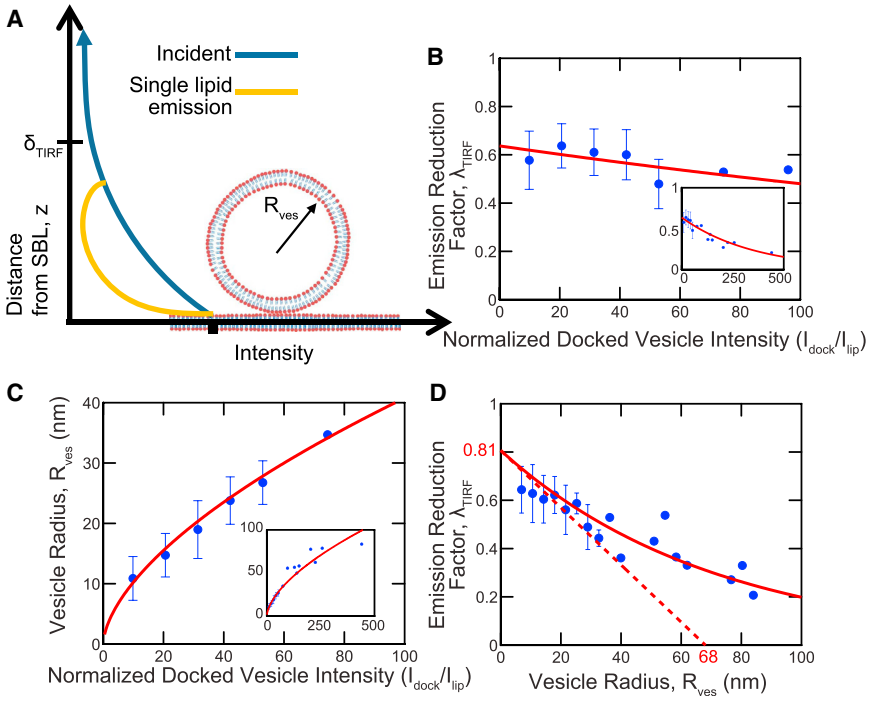

FIGURE 6 In TIRFM, the vesicle size and fluorescence reduction factor are unique functions of the docked-vesicle intensity. (*A*) The fluorescence intensity of a labeled lipid at a distance z from the SBL in a vesicle of radius R_{ves} (*lighter, yellow curve*) is the product of the decaying incident evanescent wave intensity (*darker, blue curve*) and a polarization factor due to lipid orientation. The net fluorescence reduction factor for the vesicle, λ_{TIRF}, is the average of the lighter yellow curve weighted by the number of lipids at each height. (*B* and *C*) λ_{TIRF} and R_{ves} are uniquely determined by the docked-vesicle intensity (139 fusion events; see the Supporting Material). (*B*) Values of λ_{TIRF} versus docked-vesicle intensity, I_{dock}, from this study follow a best-fit exponential $0.64\exp(-I_{dock}/350\,I_{lip})$ ($p < 0.05$) (*solid, red curve*). The bin size is 10.7. (*C*) Values of R_{ves} versus I_{dock} are well described by the best-fit power law $R_{ves} = 2.6\,(I_{dock}/I_{lip})^{0.61}$ nm ($p < 0.05$). The bin size is 10.7. (*D*) Values of λ_{TIRF} versus R_{ves} from this study. The tangent at the origin (*red dashed line*) is a linear fit to R_{ves}<35 nm points, constraining the intercept on the R_{ves} axis to be the TIRF decay length, $\delta_{TIRF} = 68$ nm (Supporting Material and Eq. S18) ($p < 0.05$). This yielded $\lambda^0_{TIRF} = 0.81$ for the limiting value of λ_{TIRF} for small vesicles, a pure polarization effect. The bin size 3.6 nm. In (*B*)–(*D*), values are shown as the mean (*dark, blue symbols*) ± SD. To see this figure in color, go online.

The underlying molecular mechanisms of fusion-pore flickering remain poorly understood. Here, we used TIRFM to study the dynamics of single SNARE-mediated fusion pores in vitro for the first time to our knowledge.

Most fusion pores reseal after slow release of lipids and soluble cargo

We simultaneously monitored soluble content marker SRB and lipid label DiD as single v-SUVs fused with t-SBLs, with ~18 ms time resolution. To within a single frame, release of the two types of label commenced simultaneously, and content release never preceded lipid release. After an initial release usually too slow to be compatible with a fully open, static pore, the pore resealed in >80% of all events, trapping some of the content labels. Our results suggest that the slow release was due to small, flickering pores. Consistent with this, using a vSUV-tSUV fusion assay, Lai et al. (52) suggested that an ~2-nm-diameter fusion pore retarded cargo release.

The size of a docked vesicle can be directly inferred from the docked-vesicle intensity in TIRFM

TIRFM is a powerful technique that selectively illuminates a small, ~100-nm-deep region adjacent to a substrate (29). Ideally, one would like to use the method to directly infer the size or location of illuminated objects from the fluorescence intensity, but this relation is not a priori known. For a docked spherical vesicle, the intensity results both from the decay of the evanescent field with distance from the substrate and from the varied orientations of labeled lipids at different locations in the vesicle whose fluorophores thus interact differently with the polarized illuminating field (Fig. 6 *A*).

Here, by tracking individual fusion events, we measured this characteristic relationship, which for a given TIRFM setup and lipid marker quantifies the relative contributions of evanescent wave decay and polarization effects to the normalized fluorescence intensity, λ_{TIRF}, as a function of vesicle radius (Fig. 6 *D*). It can be shown that the slope at the origin is $-\lambda^0_{TIRF}/\delta_{TIRF}$, where λ^0_{TIRF} is the value at zero radius and δ_{TIRF} the decay length of the evanescent excitation field, 68 nm here (see the Supporting Material). The best-fit tangent at the origin yielded $\lambda^0_{TIRF} = 0.81 \pm 0.03$, a pure polarization contribution for the label LR-PE, since evanescent field decay effects are absent as vesicle size tends to zero, and quenching effects are expected to be negligible as our lipid labeling densities are below the self-quenching threshold. λ^0_{TIRF} being less than unity shows that the evanescent field polarization (*s*-polarization here) is a worse match for labeled lipids in the vesicle, averaged over all lipid orientations in the spherical vesicle, than for lipids in the SBL.

Fusion pores mediated by SNARE proteins flicker rapidly

When vesicles fused with the SBL, vesicle-to-SBL lipid release rates were up to two orders of magnitude slower than they would be through fully open pores (Fig. S1 *C*). We conclude that pores flickered at rates $\gtrsim$ 100 Hz, the resolution limit of our measurements set by the time for a lipid to diffuse a distance of the order of the vesicle size, τ_{ves} ~ 10 ms. The small release rates could not be explained by permanently open but narrow pores, as this would require invoking pore radii, r_p, for lipid release less than the minimum value, ~2 nm, the lipid monolayer thickness. We remind the reader that our definition of the pore radius includes the inner monolayer (see Fig. S1 *A*, Eq. 1, and below). Thus, SNARE-mediated pores flicker rapidly in the absence of other fusion-machinery components.

Lipid membranes alone sustain flickering pores

We analyzed the population of slow nonspecific fusion events (32) and fusion events with protein-free SBLs, for both of which we assumed SNARE-independent fusion-pore dynamics. For all compositions but those with the highest cholesterol levels studied, pores flickered with statistics similar to those of SNARE-mediated pores: the flickering-pore openness, the fraction that were fully open, and the cholesterol dependence were similar (Fig. 4, *C* and *D*). This is consistent with previous observations of flickering pores in protein-free systems (53). This also provides further evidence that lipid diffusion is not severely restricted at the fusion pore by SNARE transmembrane domains. Our results suggest that in cells, a major component of the mechanism of fusion-pore flickering derives from the biophysical properties of the phospholipid membranes themselves, independent of SNAREs or other fusion machinery.

Cholesterol opens fusion pores by lowering the pore bending energy

Increasing amounts of cholesterol dramatically opened fusion pores (Fig. 4, *B–D*). At physiological cholesterol levels, flickering pores had a mean openness of P_o ~ 0.4, similar to the values $P_o \sim 0.3 - 0.8$ that we estimate for exocytotic pores from electrophysiological measurements (3,4,7,10). In addition, ~40% of pores were permanently open, suggesting that this may be true of exocytotic pores.

It follows that cholesterol lowers the free energy of pore formation, ΔF_{pore}, which is closely related to P_o. This trend was consistent for SNARE-mediated and SNARE-independent pores, suggesting that the origin lies in membrane energetics. Thus, adapting the model of (54), we calculated the change in the fusion-pore bending energy due to cholesterol, whose negative spontaneous curvature favors the net negative curvature of the fusion pore. Cholesterol lowered ΔF_{pore}, with a reduction of ~43 k_BT at physiological levels (Fig. S5), signifying essentially open pores, $P_o = 1$. These results can qualitatively explain the experimental trend; however, we observed that a significant fraction of pores remained flickering, suggesting additional effects beyond this simple model.

Cholesterol promotes fusion by direct membrane effects and by indirect promotion of SNARE-mediated fusion

We found that SNAREs play a very minor role in pore flickering when cholesterol is absent or at intermediate concentrations (Fig. 4, *C* and *D*), suggesting that cholesterol opens pores solely through its direct effect on membrane bending energy for these conditions. However at physiological cholesterol levels, SNAREs exerted a pronounced pore-opening effect as their presence increased the fraction of permanently open pores ~2-fold (Fig. 4 *D*). Moreover, at

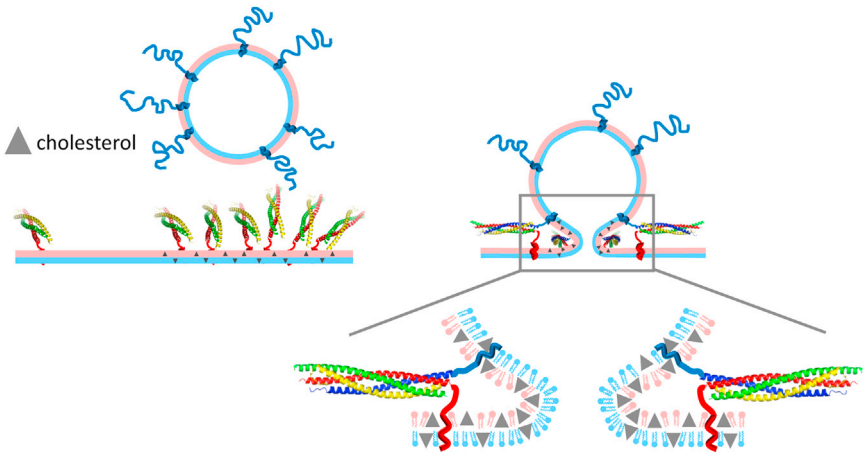

FIGURE 7 Model of promotion of SNARE-mediated fusion by cholesterol. Cholesterol (*triangles*) clusters t-SNAREs in target membranes (*left*), increasing vesicle docking rates and providing multiple t-SNAREs that are instantly available for accelerated fusion (*right*). Once initiated, the openness of the flickering pore is increased by cholesterol 1) directly, by lowering the bending energy of the pore (Fig. S5), whose negative curvature is compatible with cholesterol's large, negative spontaneous curvature, ~−0.4 nm^{-1} (55) (blow up, right); or 2) indirectly, by increasing the number of SNAREpins at the fusion pore. Increased openness stabilizes the pore and may increase content release rates and accelerate pore dilation (Fig. 1). To see this figure in color, go online.

these cholesterol levels, fusion occurred so rapidly after docking that there was insufficient time to recruit additional t-SNAREs, suggesting that t-SNAREs were preclustered at the docking site (Fig. 5 *A*), which is consistent with previous reports of cholesterol-mediated t-SNARE clustering (46–49).

A growing body of evidence suggests that cholesterol opens pores and augments fusion rates (20,23,24). Our results suggest that cholesterol facilitates exocytosis both directly, by lowering the energy to deform membranes into the severely bent shape of a fusion pore, and indirectly through its influence on SNARE proteins (Fig. 7). We propose that by clustering t-SNAREs in target membranes, cholesterol increases vesicle docking rates and increases the number of SNAREpins that cooperate to create and maintain a fusion pore, thereby increasing the openness of the pore (36). By increasing openness, these effects stabilize fusion pores, increase rates of content release, and may accelerate pore dilation.

SUPPORTING MATERIAL

Supporting Materials and Methods, Supporting Results, seven figures, and three tables are available at http://www.biophysj.org/biophysj/supplemental/S0006-3495(16)00165-X.

AUTHOR CONTRIBUTIONS

E.K. designed and performed the experiments. Z.W. and J.N. performed the single- and two-color experiments, respectively. B.O. performed the modeling analysis. B.O., B.S., and J.W. performed data analysis. B.S., G.W., E.W., and J.N. performed vesicle and lipid tracking, and Z.W. and E.K. performed vesicle tracking. D.B. designed the two-color-emission optical setup and helped E.K. to build it. D.B. and J.N. performed analysis of two-color images. B.O., B.S., and E.K. wrote the manuscript with input from others.

ACKNOWLEDGMENTS

We thank J. E. Rothman for providing equipment and lab space during the initial phase of this work and members of the O'Shaughnessy, Karatekin, and Rothman groups for helpful discussions. We thank Vladimir Polejaev (Yale West Campus Imaging Core) for building the polarized TIRF microscope used for the two-color experiments.

E.K. is supported by a Kavli Neuroscience Scholar Award from the Kavli Foundation and by National Institutes of Health grant 1R01GM108954.

SUPPORTING CITATIONS

Reference (56) is included in the Supporting Material.

REFERENCES

1. Lindau, M., and G. Alvarez de Toledo. 2003. The fusion pore. *Biochim. Biophys. Acta.* 1641:167–173.
2. Südhof, T. C., and J. E. Rothman. 2009. Membrane fusion: grappling with SNARE and SM proteins. *Science.* 323:474–477.
3. Zhou, Z., S. Misler, and R. H. Chow. 1996. Rapid fluctuations in transmitter release from single vesicles in bovine adrenal chromaffin cells. *Biophys. J.* 70:1543–1552.
4. Staal, R. G. W., E. V. Mosharov, and D. Sulzer. 2004. Dopamine neurons release transmitter via a flickering fusion pore. *Nat. Neurosci.* 7:341–346.
5. Bai, J., C. T. Wang, …, E. R. Chapman. 2004. Fusion pore dynamics are regulated by synaptotagmin*t-SNARE interactions. *Neuron.* 41:929–942.
6. Sombers, L. A., H. J. Hanchar, …, A. G. Ewing. 2004. The effects of vesicular volume on secretion through the fusion pore in exocytotic release from PC12 cells. *J. Neurosci.* 24:303–309.
7. Alvarez de Toledo, G., R. Fernández-Chacón, and J. M. Fernández. 1993. Release of secretory products during transient vesicle fusion. *Nature.* 363:554–558.
8. Han, X., C. T. Wang, …, M. B. Jackson. 2004. Transmembrane segments of syntaxin line the fusion pore of Ca^{2+}-triggered exocytosis. *Science.* 304:289–292.
9. Monck, J. R., and J. M. Fernandez. 1992. The exocytotic fusion pore. *J. Cell Biol.* 119:1395–1404.
10. Monck, J. R., G. Alvarez de Toledo, and J. M. Fernandez. 1990. Tension in secretory granule membranes causes extensive membrane transfer through the exocytotic fusion pore. *Proc. Natl. Acad. Sci. USA.* 87:7804–7808.
11. Breckenridge, L. J., and W. Almers. 1987. Final steps in exocytosis observed in a cell with giant secretory granules. *Proc. Natl. Acad. Sci. USA.* 84:1945–1949.
12. Fulop, T., S. Radabaugh, and C. Smith. 2005. Activity-dependent differential transmitter release in mouse adrenal chromaffin cells. *J. Neurosci.* 25:7324–7332.
13. He, L., X. S. Wu, …, L. G. Wu. 2006. Two modes of fusion pore opening revealed by cell-attached recordings at a synapse. *Nature.* 444:102–105.
14. Klyachko, V. A., and M. B. Jackson. 2002. Capacitance steps and fusion pores of small and large-dense-core vesicles in nerve terminals. *Nature.* 418:89–92.
15. Lisman, J. E., S. Raghavachari, and R. W. Tsien. 2007. The sequence of events that underlie quantal transmission at central glutamatergic synapses. *Nat. Rev. Neurosci.* 8:597–609.
16. Fang, Q., K. Berberian, …, M. Lindau. 2008. The role of the C terminus of the SNARE protein SNAP-25 in fusion pore opening and a model for fusion pore mechanics. *Proc. Natl. Acad. Sci. USA.* 105:15388–15392.
17. Breckenridge, W. C., G. Gombos, and I. G. Morgan. 1972. The lipid composition of adult rat brain synaptosomal plasma membranes. *Biochim. Biophys. Acta.* 266:695–707.
18. Takamori, S., M. Holt, …, R. Jahn. 2006. Molecular anatomy of a trafficking organelle. *Cell.* 127:831–846.
19. Traynor, A. E., D. Schubert, and W. R. Allen. 1982. Alterations of lipid metabolism in response to nerve growth factor. *J. Neurochem.* 39:1677–1683.
20. Linetti, A., A. Fratangeli, …, P. Rosa. 2010. Cholesterol reduction impairs exocytosis of synaptic vesicles. *J. Cell Sci.* 123:595–605.
21. Wang, N., C. Kwan, …, F. W. Tse. 2010. Influence of cholesterol on catecholamine release from the fusion pore of large dense core chromaffin granules. *J. Neurosci.* 30:3904–3911.
22. Zhang, Z., and M. B. Jackson. 2010. Membrane bending energy and fusion pore kinetics in Ca^{2+}-triggered exocytosis. *Biophys. J.* 98:2524–2534.
23. Tong, J., P. P. Borbat, …, Y. K. Shin. 2009. A scissors mechanism for stimulation of SNARE-mediated lipid mixing by cholesterol. *Proc. Natl. Acad. Sci. USA.* 106:5141–5146.
24. Biswas, S., S.-R. Yin, …, J. Zimmerberg. 2008. Cholesterol promotes hemifusion and pore widening in membrane fusion induced by influenza hemagglutinin. *J. Gen. Physiol.* 131:503–513.

25. Curran, M. J., F. S. Cohen, …, J. Zimmerberg. 1993. Exocytotic fusion pores exhibit semi-stable states. *J. Membr. Biol.* 133:61–75.

26. Spruce, A. E., L. J. Breckenridge, …, W. Almers. 1990. Properties of the fusion pore that forms during exocytosis of a mast cell secretory vesicle. *Neuron.* 4:643–654.

27. B. Sackmann, and E. Neher, editors 1995. Single-Channel Recording. Plenum Press, New York.

28. Chizmadzhev, Y. A., F. S. Cohen, …, J. Zimmerberg. 1995. Membrane mechanics can account for fusion pore dilation in stages. *Biophys. J.* 69:2489–2500.

29. Axelrod, D. 2008. Total internal reflection fluorescence microscopy. *Methods Cell Biol.* 89:169–221.

30. Cremona, O., and P. De Camilli. 2001. Phosphoinositides in membrane traffic at the synapse. *J. Cell Sci.* 114:1041–1052.

31. Karatekin, E., and J. E. Rothman. 2012. Fusion of single proteoliposomes with planar, cushioned bilayers in microfluidic flow cells. *Nat. Protoc.* 7:903–920.

32. Karatekin, E., J. Di Giovanni, …, J. E. Rothman. 2010. A fast, single-vesicle fusion assay mimics physiological SNARE requirements. *Proc. Natl. Acad. Sci. USA.* 107:3517–3521.

33. Kyoung, M., Y. Zhang, …, A. T. Brunger. 2013. Studying calcium-triggered vesicle fusion in a single vesicle-vesicle content and lipid-mixing system. *Nat. Protoc.* 8:1–16.

34. Hung, W.-C., M.-T. Lee, …, H. W. Huang. 2007. The condensing effect of cholesterol in lipid bilayers. *Biophys. J.* 92:3960–3967.

35. Smith, M. B., E. Karatekin, …, D. Vavylonis. 2011. Interactive, computer-assisted tracking of speckle trajectories in fluorescence microscopy: application to actin polymerization and membrane fusion. *Biophys. J.* 101:1794–1804.

36. Shi, L., Q. T. Shen, …, F. Pincet. 2012. SNARE proteins: one to fuse and three to keep the nascent fusion pore open. *Science.* 335:1355–1359.

37. Chernomordik, L. V., G. B. Melikyan, and Y. A. Chizmadzhev. 1987. Biomembrane fusion: a new concept derived from model studies using two interacting planar lipid bilayers. *Biochim. Biophys. Acta.* 906: 309–352.

38. Honigmann, A., G. van den Bogaart, …, R. Jahn. 2013. Phosphatidylinositol 4,5-bisphosphate clusters act as molecular beacons for vesicle recruitment. *Nat. Struct. Mol. Biol.* 20:679–686.

39. Liu, T., W. C. Tucker, …, J. C. Weisshaar. 2005. SNARE-driven, 25-millisecond vesicle fusion in vitro. *Biophys. J.* 89:2458–2472.

40. Durning, C., and B. O'Shaughnessy. 1988. Diffusion controlled reactions at an interface. *J. Chem. Phys.* 88:7117–7128.

41. Bowen, M. E., K. Weninger, …, S. Chu. 2004. Single molecule observation of liposome-bilayer fusion thermally induced by soluble *N*-ethyl maleimide sensitive-factor attachment protein receptors (SNAREs). *Biophys. J.* 87:3569–3584.

42. Zimmerberg, J., R. Blumenthal, …, S. J. Morris. 1994. Restricted movement of lipid and aqueous dyes through pores formed by influenza hemagglutinin during cell fusion. *J. Cell Biol.* 127:1885–1894.

43. Tse, F. W., A. Iwata, and W. Almers. 1993. Membrane flux through the pore formed by a fusogenic viral envelope protein during cell fusion. *J. Cell Biol.* 121:543–552.

44. Chen, Y. D., R. J. Rubin, and A. Szabo. 1993. Fluorescence dequenching kinetics of single cell-cell fusion complexes. *Biophys. J.* 65: 325–333.

45. Razinkov, V. I., G. B. Melikyan, and F. S. Cohen. 1999. Hemifusion between cells expressing hemagglutinin of influenza virus and planar membranes can precede the formation of fusion pores that subsequently fully enlarge. *Biophys. J.* 77:3144–3151.

46. Lang, T., D. Bruns, …, R. Jahn. 2001. SNAREs are concentrated in cholesterol-dependent clusters that define docking and fusion sites for exocytosis. *EMBO J.* 20:2202–2213.

47. Barg, S., M. K. Knowles, …, W. Almers. 2010. Syntaxin clusters assemble reversibly at sites of secretory granules in live cells. *Proc. Natl. Acad. Sci. USA.* 107:20804–20809.

48. van den Bogaart, G., K. Meyenberg, …, R. Jahn. 2011. Membrane protein sequestering by ionic protein-lipid interactions. *Nature.* 479: 552–555.

49. Milovanovic, D., A. Honigmann, …, R. Jahn. 2015. Hydrophobic mismatch sorts SNARE proteins into distinct membrane domains. *Nat. Commun.* 6:5984.

50. Breckenridge, L. J., and W. Almers. 1987. Currents through the fusion pore that forms during exocytosis of a secretory vesicle. *Nature.* 328:814–817.

51. Zimmerberg, J., M. Curran, …, M. Brodwick. 1987. Simultaneous electrical and optical measurements show that membrane fusion precedes secretory granule swelling during exocytosis of beige mouse mast cells. *Proc. Natl. Acad. Sci. USA.* 84:1585–1589.

52. Lai, Y., J. Diao, …, Y. K. Shin. 2013. Fusion pore formation and expansion induced by Ca^{2+} and synaptotagmin 1. *Proc. Natl. Acad. Sci. USA.* 110:1333–1338.

53. Chanturiya, A., L. V. Chernomordik, and J. Zimmerberg. 1997. Flickering fusion pores comparable with initial exocytotic pores occur in protein-free phospholipid bilayers. *Proc. Natl. Acad. Sci. USA.* 94: 14423–14428.

54. Kozlov, M. M., S. L. Leikin, …, Y. A. Chizmadzhev. 1989. Stalk mechanism of vesicle fusion. Intermixing of aqueous contents. *Eur. Biophys. J.* 17:121–129.

55. Chen, Z., and R. P. Rand. 1997. The influence of cholesterol on phospholipid membrane curvature and bending elasticity. *Biophys. J.* 73:267–276.

56. Wagner, M. L., and L. K. Tamm. 2001. Reconstituted syntaxin1a/SNAP25 interacts with negatively charged lipids as measured by lateral diffusion in planar supported bilayers. *Biophys. J.* 81:266–275.

Biophysical Journal, Volume *110*

Supplemental Information

Cholesterol Increases the Openness of SNARE-Mediated Flickering Fusion Pores

Benjamin S. Stratton, Jason M. Warner, Zhenyong Wu, Joerg Nikolaus, George Wei, Emma Wagnon, David Baddeley, Erdem Karatekin, and Ben O'Shaughnessy

Biophysical Journal

Supporting Material

Cholesterol Increases the Openness of SNARE-Mediated Flickering Fusion Pores

Benjamin S. Stratton,[1] Jason M. Warner ,[1] Zhenyong Wu,[2,3] Joerg Nikolaus,[2,3] George Wei,[1] Emma Wagnon,[1] David Baddeley,[3,4] Erdem Karatekin,[2,3,5,6,*] and Ben O'Shaughnessy[1,*]

[1]Department of Chemical Engineering, Columbia University, New York, New York; [2]Department of Cellular and Molecular Physiology, Yale University, School of Medicine, New Haven, Connecticut; [3]Nanobiology Institute, Yale University, West Haven, Connecticut; [4]Department of Cell Biology and [5]Department of Molecular Biophysics and Biochemistry, Yale University, New Haven, Connecticut; and [6]Laboratoire de Neurophotonique, Université Paris Descartes, Centre National de la Recherche Scientifique (CNRS) UMR8250, Paris, France

*Correspondence: bo8@columbia.edu; erdem.karatekin@yale.edu

Decomposition of the docking-to-fusion delay time distribution into a fast and a slow component

For each fusion event, following docking of a vesicle onto the SBL fusion occurred after a delay time τ_{delay} (Fig. **2**B, C). We measured τ_{delay} from the TIRF signal and for each lipid composition we constructed the distribution of delay times, represented as the survivor function $S(\tau_{\mathrm{delay}})$, the probability fusion has not occurred after a time τ_{delay} (Fig. **S2**E). From these distributions we found that there are two populations of fusion events: a fast-fusing population and a slowly fusing population with significantly longer delay times, similarly to ref. (1). Following ref. (1) we interpreted the fast fusers as being SNARE-dependent, and the slow fusers as originating in non-specific events and involving fusion pores whose dynamics were not controlled by SNAREpins. This enabled us to measure the effects of SNARE proteins on flickering fusion pore dynamics, and to study by comparison the dynamics of fusion pores that are apparently controlled only by the lipid membranes independently of SNAREs, consistent with ref. (1).

The survivor distributions were well fit by mixed exponentials of the form $S(\tau_{\mathrm{delay}}) = a\exp(-\tau_{\mathrm{delay}}/\overline{\tau}_{\mathrm{delay}}) + (1-a)\exp(-\tau_{\mathrm{delay}}/\overline{\tau}_{\mathrm{ns}})$ where a is the amplitude of the fast fusing component and is interpreted as the fraction of vesicles which fuse in a SNARE-mediated manner, $\overline{\tau}_{\mathrm{delay}}$ is the mean docking-to-fusion delay time for SNARE-mediated fusion, and $\overline{\tau}_{\mathrm{ns}}$ is the mean delay time for non-specific fusion. Fits were obtained using a maximum likelihood estimate using Matlab's Statistics Toolbox. $\overline{\tau}_{\mathrm{ns}}$ was in the range $\sim 2-3$ s for all compositions, ~10 times greater than typical mean delay times for specific SNARE-mediated events.

Method to identify events as fast or slow. We determined a maximum cutoff time for the specific SNARE-mediated events, and defined all events with τ_{delay} less (greater) than this time to be specific (non-specific) events. The cutoff time was determined as follows. As the parameter a represents the fraction of fusion events which are SNARE-mediated, we varied the cutoff time until the fraction of fusion events below this cutoff time matched a from the double exponential fit. For self-consistency, we checked that the cutoff time was larger than the mean value of the delay time for the fast fusers and smaller than the mean value of the delay time for the slow

fusers. The cutoff times we find, ~70-600 ms (Fig. **S2**E), are ~2-6-fold greater than $\overline{\tau}_{\mathrm{delay}}$ and ~4-fold smaller than $\overline{\tau}_{\mathrm{ns}}$.

The statistics of fusion events between v-SUVs and protein-free SBLs are similar to those for the slow component of fusion events between v-SUVs and t-SBLs. We also examined fusion events between protein-free SBLs (pf-SBLs) and v-SNARE containing SUVs (v-SUVs). To test that the slow component of the fusion events between t-SNARE containing SBLs (t-SBLs) and v-SUVs represented events for which the fusion pore dynamics were SNARE-independent, we compared $\overline{\tau}_{\mathrm{ns}}$ to $\overline{\tau}_{\mathrm{pf}}$, the mean value of the delay time for pf-SBL/v-SUV fusion events. For membranes with 45% (10%) cholesterol in the SUV (SBL) we found $\overline{\tau}_{\mathrm{pf}} \sim 1.9$ s, statistically indistinguishable from $\overline{\tau}_{\mathrm{ns}}$ for the same composition, Fig. 5A ($p>0.05$). Similarly, for the same composition the openness $P_0 \sim 0.05 \pm 0.02$ of pf-SBL/v-SUVs fusion pores was statistically indistinguishable from the pore openness for the slow component of the t-SBL/v-SUV fusion events ($P>0.05$, see non-specific events in Fig. 4C).

These observations are consistent with the hypothesis that the fusion pore dynamics of the slow component of t-SBL/v-SUV events are determined by the physical properties of the lipid bilayers.

Properties of single fluorescent lipids in the SBL

In the main text (*SNARE-mediated fusion pores flicker or are permanently open*, in Results) we fit the predicted total intensity time course, eq. 3, to the measured integrated intensity time course $I_{\mathrm{tot}}(t)$ for each fusion event to determine the pore openness and vesicle size (Fig. 4). In order to perform this fit, we required three single lipid properties: the single fluorescent lipid intensity I_{lip} in the SBL, the fluorescent lipid bleaching time in the SBL τ_{bleach}, and the single lipid diffusivity D_{lip} (Fig. **S2**). Almost all fluorescent spots released into the SBL upon fusion remained bright for a period and then suddenly darkened (bleached) in a single frame, consistent with these spots being single fluorescent lipids. In this way, for each lipid we made a 'digital' measurement of the bleaching time. We confined our single lipid analysis to those which

bleached in one step in this manner. Fluorescent lipids were tracked using SpeckleTrackerJ (2), and further analysis was performed using Matlab.

Measurement of single fluorescent lipid intensity, $I_{\mathbf{lip}}$. We measured the intensity of a single lipid by measuring the average change of intensity upon bleaching. We take the average of the total intensity of a lipid in an area $3x3$ pixels ($0.80\ x\ 0.80\ \mu m^2$) centered on the lipid, time-averaged over the final 15 frames for which the lipid fluoresced. We measured the background intensity in the same location where the lipid bleached, over the 15 frames following bleaching. The latter was subtracted from the former to determine the intensity of the individual lipid. We then averaged each of these individual lipid intensities over ~40 lipids to determine the mean single lipid intensity I_{lip} for a given movie, ~1 min in duration (i.e. Fig. **S2**A). All analysis of events from that movie used the measured single lipid intensity from that movie.

Measurement of single lipid diffusion coefficient, $D_{\mathbf{lip}}$. We calculated the mean square displacement (MSD) for lipid trajectories lasting $\gtrsim$ 1.5 seconds and determined the best fit linear relation of MSD vs. t over time windows ranging from one to 10 frames ($t_{\mathrm{frame}} \approx$ 17 ms or 31 ms) to sample a full range of the trajectory. A sample of 7 of these MSD curves is shown in Fig. **S2**B. We then calculated the diffusion constant from $\mathrm{MSD} = MSD(0) + 4\,D_{\mathrm{lip}}\,t$ for each analyzed trajectory. We report a mean $\pm$ SEM D_{lip} averaged from ~20 analyzed lipid trajectories for each lipid composition, Table **S3**. The MSD was calculated in Matlab.

Measurement of lipid bleaching time in the SBL, $\tau_{\mathbf{bleach}}$. We measured the lipid bleaching time τ_{bleach} by determining the total duration of single lipid trajectories and then calculating the survivor function $f_{\mathrm{fluor}}(t)$ describing many such trajectories. We fit a decaying exponential to the survivor function $f_{\mathrm{fluor}}(t) = e^{-t/\tau_{\mathrm{bleach}}}$ (Fig. **S2C**). Approximately 50 bleaching episodes were used to calculate the survivor function in each movie. The uncertainty reported is the 95% confidence interval from the fitting routine.

The bleaching rate in the vesicle is much slower than that in the SBL. Our measurements of single lipid bleaching were for lipids in the SBL. To determine bleaching rates for lipids in vesicles (expected to be lower since the fluorescence emission is lower) we measured the bleaching time of entire vesicles $\tau_{\mathrm{bleach}}^{\mathrm{ves}}$ for ~ 30 vesicles that did not fuse per movie. We measured $\tau_{\mathrm{bleach}}^{\mathrm{ves}}$ from the best fit exponential $I_{\mathrm{tot}}(t) = I_{\mathrm{o}} \exp(-t/\tau_{\mathrm{bleach}}^{\mathrm{ves}})$ (Fig. S2D). I_{tot} is

the spatially integrated intensity over a box of size 15x15 pixels centered on the unfused vesicle, with the background subtracted off. Repeating this for each movie, we found that the bleaching time in vesicles is ~5-8-fold greater than the bleaching time in the SBL. Thus, when we used our model to calculate the fluorescence intensity versus time, $I_{tot}(t)$, we neglected fluorescent bleaching of lipids in the vesicle (eqs. **3, 4**).

Analysis of individual fusion events.

For each fusion event, we measured the total intensity versus time *t*, $I_{\mathrm{tot}}(t)$ (Fig. 2B and C). To do this, we measured the integrated intensity by drawing a square region of interest of size $30x30$ pixels. We use a box of this size to ensure that all of the lipids remain in the box for the duration of the measurement, 1.6 s. We analyzed fusion events with longer release times by manually drawing larger boxes based on the specific fusion event. Fusing vesicles were well spaced enough that we did not have to account for significant background lipid diffusion into the region of interest.

In TIRFM the evolving fluorescence intensity following a SUV-SBL fusion event provides a high time resolution readout of lipid transfer. As described in the main text, when lipids diffuse from a vesicle into the SBL through the walls of a fusion pore a rapid increase in fluorescence intensity is observed due to the spatial decay of the intensity of the incident evanescent wave, and the change in mean lipid orientation when a lipid transfers to the planar SBL from the spherical SUV which alters the coupling to the polarized evanescent wave. The increase in fluorescence is instantaneous upon transfer of a labeled lipid into the SBL and thus provides a very sensitive measure of the fraction of dye transferred between the fusing membranes as a function of time, with temporal resolution limited only by acquisition frame rates (~100 Hz, which is in turn limited by the exposure time needed to detect single fluorophores). In conjunction with a mathematical model of release through a flickering pore, this enabled us to accurately measure SUV-to-SBL lipid release times τ_{release}. A fitting procedure using the mathematical model was needed because the lipid release kinetics are convoluted with bleaching kinetics (Fig. 2C).

By comparison the spread of the dye from the fusion site to a distance larger than the optical resolution (~250 nm) would take 60 ms or longer (taking D_{lip}=1 $\mu m^2 s^{-1}$), too slow to measure typical release times. In a previous work where we employed the present SUV-SBL fusion assay, but used far-field fluorescence microscopy rather than TIRFM, the signal of fusion was taken to be this spread of lipids from the fusion site, quantified by the time course of the width of a two-dimensional Gaussian profile fit to the image sequence representing a fusing vesicle (1).

A different kind of resolution limit determines the minimum flickering frequency our method can access. When a flickering pore opens (Fig. S1A), if it remains open for longer than the time for all labelled lipids to diffuse out of the vesicle through the open pore, the signal will be lost before completion of a single flicker cycle. This diffusion time is approximately τ_{ves}, the lipid diffusion time for a distance of order the vesicle size (multiplied by a logarithmic factor of order unity involving the pore diameter). Thus when we observe a pore openness <1, indicating that the release time exceeds τ_{ves}, the most we can say is that the flickering frequency is higher than this lower limit. Given τ_{ves}~ 10ms for a typical vesicle size, it follows that the pores we measure flicker at frequencies $\gtrsim 100$ Hz. A similar limitation holds for amperometry, once the contents have been released, the pore may continue to flicker without being observed.

Dependence of fusion statistics on vesicle size

Fusion pore statistics do not depend on vesicle size. Over the vesicle size range ($10\,nm \lesssim R_{ves} \lesssim 80\,nm$) and lipid compositions studied, our data did not reveal correlations between vesicle size and either docking-to-fusion delay times, pore openness P_o or the fraction of pores that were permanently open (Fig. **S4**A-C).

Fusion probability does not depend on vesicle size. A fraction of vesicles dock but do not fuse within the time the labelled lipids in the vesicle have completely bleached. Thus we sought to determine whether these vesicles followed a different size distribution to vesicles that fused, as this would suggest size-dependence in the fusion mechanism.

For these events where fusion does not occur we could not use our usual procedure to measure vesicle size, which is based on fitting our model to a fluorescence intensity versus time curve

I_{tot}(t) during a fusion event. Thus, to obtain the size distribution of such vesicles, we measured the docked vesicle intensity I_{dock} (Fig. 2**C**) and to deduce the vesicle radius R_{ves} we used the best fit power law relation $R_{\mathrm{ves}} = 2.6\left(I_{\mathrm{dock}}/I_{\mathrm{lip}}\right)^{0.61}$ obtained from the assembled data from this study (Fig. **6C**).

We then compared this distribution of non-fusers to the vesicle size distribution for vesicles that underwent SNARE-mediated fusion. The comparison showed that the size distributions were statistically indistinguishable (Fig. **S4D**).

Calculation of relation between pore openness and lipid release time

In the main text ("Fusion pore openness P_{o} is quantitatively related to lipid release time τ_{release}" in Results) we presented results to a mathematical model of diffusion of labeled lipids from the membrane of a vesicle through a flickering fusion pore into the SBL membranes, eqs. 1, 3, and 4. Here, we describe the derivation of these results, specifically the results for P_{o} as a function of vesicle area A_{ves} and lipid release time τ_{release} (eq. 1), and the time dependent TIRF intensity emission $I_{\mathrm{tot}}(t)$ for both a flickering pore and a permanently open pore (eqs. 3 and 4 of the main text).

We will show below that $\phi_{ves}(t)$ decays exponentially in time for a flickering pore. In parallel, we will show that for the special case of a fully open pore the release kinetics are instead of power law form, $\phi_{\mathrm{ves}} \sim 1/t$ (eq. 3).

The flickering pore is open for a fraction P_{o} of the time and closed for a fraction $1 - P_{\mathrm{o}}$ of the time. The starting point of the model is the time evolution of the density of labelled lipids in the vesicle, $n(\boldsymbol{x}, \boldsymbol{t})$ and in the SBL, $\rho(\boldsymbol{r}, \boldsymbol{t})$ (Fig. **S1**A).

$$\partial \mathrm{n}/\,\partial \mathrm{t} = D_{\mathrm{lip}}\nabla^2 n \;-\; Q(t)\delta(\boldsymbol{x}), \qquad \partial \rho/\,\partial \mathrm{t} = D_{\mathrm{lip}}\nabla^2 \rho \;+\; Q(t)\delta(\boldsymbol{r}), \qquad \textbf{S1}$$

where D_{lip} is the lipid diffusivity. From these fields, we calculate the fraction of labelled lipids remaining in the vesicle, $\phi_{\mathrm{ves}}(t)$. The driving force for lipid release from the vesicle into the SBL is the density difference across the fusion pore, $n_0(t) - \rho_0(t)$. The lipid release rate $Q(t)$ is the product of this density difference and the pore transmission coefficient k_{pore}

$$Q(t) = \; k_{\mathrm{pore}}\{n(0,t) - \rho(0,t)\}, \qquad d\phi_{ves}/dt \; = -Q(t)/n_0 A_{\mathrm{ves}}\,, \qquad \textbf{S2}$$

where k_{pore} is the pore transmission coefficient and n_{o} the initial density of labeled lipids in the vesicle of area A_{ves}. For simplicity, we take the pore as a cylinder of height b and radius r_{p}, commonly assumed in the interpretation of pore conductances (3-6). The release rate is then the flux through a cylindrical membrane tube of cross-sectional length $2\pi r_{\mathrm{p}}$, i.e.

$$k_{\mathrm{pore}} = P_{\mathrm{o}}\, D_{\mathrm{lip}} 2\pi \mathrm{r_p}/\mathrm{b}. \qquad \textbf{S3}$$

Note that k_{pore} is reduced by the pore openness, P_{o}, which for a two-state (open/closed) pore is the fraction of the time the flickering pore is in the open state. More generally, for a pore whose size changes continuously up to some maximum size in the fully open state, P_{o} is the mean pore radius relative to the maximum value.

We consider two cases: an infrequently open flickering pore (eq. 1) and a permanently open pore (eq. 3). We then calculate the total TIRF intensity as a function of time, $I_{\mathrm{tot}}(t)$, for each case, allowing us to extract lipid release times τ_{release}, vesicle sizes R_{ves}, and pore openness P_{o} for individual fusion events.

The solutions to eq. S1 can be written:

$$\begin{aligned} n(\boldsymbol{x},\boldsymbol{t}) &= \mathbf{n}_{\mathrm{a}} - \textstyle\int_0^t \boldsymbol{dt'}\mathbf{Q}(\mathbf{t'})\mathbf{G_s}(\mathbf{0},\mathbf{x},\mathbf{t}-\mathbf{t'}) \\ \rho(\mathbf{r},\mathbf{t}) &= \textstyle\int_0^t \boldsymbol{dt'}\mathbf{Q}(\mathbf{t'})\mathbf{G}(\mathbf{0},\mathbf{r},\mathbf{t}-\mathbf{t'}) \end{aligned}, \qquad \textbf{S4}$$

where $\mathbf{G_s}(\mathbf{x'},\mathbf{x},\mathbf{t})$ is the Green's function of the diffusion equation in the vesicle, the probability a lipid in the vesicle at $\mathbf{x'}$ diffuses to $\mathbf{x}$ a time $\mathbf{t}$ later, and $\mathbf{G}(\mathbf{r'},\mathbf{r},\mathbf{t})$ is the same for the SBL. Setting $\mathbf{r}=\mathbf{x}=0$ and including eq. S1 and S2 gives:

$$\begin{aligned} n_0(t) &= n_{\mathrm{a}} - \textstyle\int_0^t dt' g(t-t') \\ \rho_0(t) &= \textstyle\int_0^t dt' Q(t') S(t-t') \\ Q(t) &= k_{\mathrm{pore}}\left(n_0(t) - \rho_0(t)\right) \end{aligned} \qquad \textbf{S5}$$

where g and S are the return probabilities for the vesicle and the SBL respectively, namely the Green's functions evaluated at $\mathbf{x}=\mathbf{x'}$ and $\mathbf{r}=\mathbf{r'}$, respectively, and n_0, ρ_0 denote the densities at $\mathbf{x}$=0 and $\mathbf{r}$=0, respectively. In general, k_{pore} fluctuates with time. However, since measured flickering timescales are far less than the lipid release time we assumed that k_{pore} can be treated as a constant, the effective time-averaged value.

Laplace transforming $t \to E$, the solution is:

$$
\begin{aligned}
Q &= \frac{k_{\mathrm{pore}} n_{\mathrm{a}}}{E\left[1+k_{\mathrm{pore}}\left(g(E)+S(E)\right)\right]}\,, \\
\rho_0 &= \frac{k_{\mathrm{pore}} n_{\mathrm{a}} S}{E\left[1+k_{\mathrm{pore}}\left(g(E)+S(E)\right)\right]}\,, \\
n_0/n_{\mathrm{a}} &= \frac{k_{\mathrm{pore}} S}{E\left[1+k_{\mathrm{pore}}\left(g(E)+S(E)\right)\right]}\,,
\end{aligned}
\qquad \textbf{S6}
$$

where $Q(E), \rho_{\mathrm{o}}(E), n_0(E), g(E), S(E)$ are all functions of E. Note that G is a simple 2D Gaussian describing free lipid diffusion in the SBL. Thus, $S(t) = 1/4\pi D_{\mathrm{lip}}\, t$, and a crude approximation of its Laplace transform is $S(E) \approx \left(1/D_{\mathrm{lip}}\right) \ln(1/E t_{\mathrm{b}})$ where $t_{\mathrm{b}} = b^2/D_{\mathrm{lip}}$ and b is a pore cut-off scale.

Lipid release through a flickering fusion pore. If $k_{\mathrm{pore}} \ll D_{\mathrm{lip}}$, then $S(E) \ll 1/k_{\mathrm{pore}}$ for any $E > t_{\mathrm{b}}^{-1} e^{1/\epsilon}$, where $\epsilon = k_{\mathrm{pore}}/D_{\mathrm{lip}}$. Thus for small enough ϵ, for all relevant E we can delete the $k_{\mathrm{pore}}\, S$ terms in eq. S3. In addition, we can replace $g(E) \approx 1/E A_{\mathrm{ves}}$ with its form for small E ($E < 1/\tau_{\mathrm{ves}}$) reflecting the fact that on time scales greater than τ_{ves} a point source uniformly covers the vesicle. We justify this below. Thus, eq. **S5** gives:

$$
\begin{aligned}
n_0 &= \frac{n_{\mathrm{a}}}{E + k_{\mathrm{pore}}/A_{\mathrm{ves}}} \\
\rho_0 &= \frac{k_{\mathrm{pore}} n_{\mathrm{a}} S}{E + k_{\mathrm{pore}}/A_{\mathrm{ves}}} \\
Q &= k_{\mathrm{pore}} n_0
\end{aligned}
\qquad \textbf{S7}
$$

The solution is $n_0(t) = n_a \exp(-t/\tau_{\mathrm{release}})$ where $\tau_{\mathrm{release}} = A_{\mathrm{ves}}/k_{\mathrm{pore}}$. Using the expression for k_{pore} in eq. S3, we arrive at the expression for pore openness P_{o} in terms of τ_{release} and A_{ves} of eq. 1 of the main text. Using the expression for Q in eq. S7 in eq. S2 gives

$$
\phi_{\mathrm{ves}} = \exp(-t/\tau_{\mathrm{release}}) \qquad \textbf{S8}
$$

In this limit, $n(x,t) \approx n_0(t)$ is uniform because the release time greatly exceeds the vesicle diffusion time (since $\tau_{\mathrm{release}}/\tau_{\mathrm{ves}} = 1/\epsilon \gg 1$). Further, the fraction released by time τ_{ves} is thus very small. Since $g(t)$ assumes its long time form ($1/A_{\mathrm{ves}}$) for times $t > \tau_{\mathrm{ves}}$, this justifies our replacing $g(E)$ with its long time form to obtain eq. **S8**: these are the only time scales relevant to the decay of ϕ_{ves}.

TIRF intensity time course through a flickering fusion pore. In this subsection we derive the expression of eq. 2 in the main text for the time-dependent total fluorescence intensity of labelled

lipids during a fusion event. The total intensity I_{tot} is the sum of the intensity of lipids in the vesicle and the intensity of lipids released into the SBL. The calculation of this quantity rests on three principal features. (i) When a lipid in a SUV is released into the SBL its emission increases by a factor $1/\lambda_{\mathrm{TIRF}}$. (ii) We ignore lipid bleaching in SUVs, being significantly slower than for lipids in the SBL (Figs. **S3C**, **D**). (iii) When a lipid is released through a flickering pore into the SBL, in this small k_{pore} limit that defines a flickering pore it is very unlikely to diffuse back into the vesicle. This follows from the fact that $n_0 \ll \rho_0$ in this flickering pore limit, for which $\mathrm{k}_{\mathrm{pore}}\, S \ll 1$ (see eq. S7), so the current of lipids is almost completely unidirectional from SUV to SBL (see eq. 2 of main text).

The total intensity for a vesicle is the sum of the contributions of fluorescent lipids which remain in the vesicle, and those that are in the SBL and have not yet bleached. The initial number of lipids in the vesicle is $N_{\mathrm{ves}}^{\mathrm{a}} = n_{\mathrm{a}} A_{\mathrm{ves}}$. The number of lipids in the vesicle decays as eq. S8, that is $N_{\mathrm{ves}}(t) = N_{\mathrm{ves}}^{\mathrm{a}} \exp(-t/\tau_{\mathrm{release}})$. The rate of fluorescent lipid addition to the SBL is the same magnitude as the rate of lipid release from the vesicle. Thus, the number of fluorescent lipids in the SBL, $N_{\mathrm{SBL}}(t)$, obeys

$$\frac{dN_{SBL}}{dt} = \frac{N_{\mathrm{ves}}(t)}{\tau_{\mathrm{release}}} - \frac{N_{\mathrm{SBL}}(t)}{\tau_{\mathrm{bleach}}},$$

where we used the fact that for this flickering pore case spatial variations in density in the vesicle can be ignored ($n(x,t) \approx n_0(t) = N_{\mathrm{ves}}(t)/A_{\mathrm{ves}}$). The solution is

$$N_{\mathrm{SBL}}(t) = \frac{N_{\mathrm{ves}}^{\mathrm{a}}\left(e^{-t/\tau_{\mathrm{bleach}}} - e^{-t/\tau_{\mathrm{release}}}\right)}{(1 - \tau_{\mathrm{release}}/\tau_{\mathrm{bleach}})}. \qquad \textbf{S9}$$

Hence the total intensity is given by

$$I_{\mathrm{tot}}(t) = I_{\mathrm{lip}} \lambda_{\mathrm{TIRF}} N_{\mathrm{ves}}(t) + I_{\mathrm{lip}} N_{\mathrm{SBL}}(t) \qquad \textbf{S10}$$

where $N_{SBL}(t)$ is given by eq. S9 and $N_{\mathrm{ves}}(t) = N_{\mathrm{ves}}^{\mathrm{a}} \exp(-t/\tau_{\mathrm{release}})$. As the vesicle intensity at the instant of fusion is $I_{\mathrm{fus}} = I_{\mathrm{lip}} \lambda_{\mathrm{TIRF}} N_{\mathrm{ves}}^{\mathrm{a}}$, we obtain $I_{\mathrm{tot}}(t)$ in terms of τ_{release}, λ_{TIRF}, and τ_{bleach} of eq. 2 in the main text by plugging eq. **S9** and the expression for $N_{\mathrm{ves}}(t)$ above into eq. **S8**.

The case of a permanently open pore. For a fully open pore, $P_{\mathrm{o}} = 1$, eq. S3 tells us that $k_{\mathrm{pore}} = D_{\mathrm{lip}} 2\pi r_{\mathrm{p}}/b$. Thus k_{pore} is of order D_{lip} ($\epsilon \approx 1$), and $k_{\mathrm{pore}}\, S(E) \gg 1$ for all $E \gg t_{\mathrm{b}}^{-1}$, ie for all relevant E. Thus from eq. **S6**

$$\rho_o \approx n_0 \approx n_{\mathrm{a}} A_{\mathrm{ves}} S(E) \qquad \textbf{S11}$$

Consider the behavior for $E \ll 1/\tau_{\mathrm{ves}}$. On these time scales $ES < 1/A_{\mathrm{ves}}$ and we have

$$\rho_{\mathrm{o}}(E) \approx n_0(E) \approx n_{\mathrm{a}} A_{\mathrm{ves}} S(E), (E < 1/\tau_{\mathrm{ves}}) \qquad \textbf{S12}$$

Thus $n_0(t)$ decays as $S(t) = 1/(4\,\pi D_{\mathrm{lip}} t)$, and $\phi_{\mathrm{ves}}(t) \approx n_0(t)/n_{\mathrm{a}} = A_{\mathrm{ves}} S(t)$. Hence we obtain eq. 4 of the main text $\phi_{\mathrm{ves}}(t) = \tau_{\mathrm{ves}}/t$. The form of the net TIRF signal $I_{\mathrm{tot}}(t)$ is modified from eq. 3 of the main text. Unlike flickering pores, reverse diffusion is significant through an open pore: typical lipids transit the fusion pore many times and lipids which have bleached will reenter the vesicle, just as fluorescing lipids will. Thus, all lipids have equal probability of bleaching and the predicted TIRF fluorescence intensity $I_{\mathrm{tot}}(t)$ for permanently open pores is thus eq. 4 of the main text.

Calculation of the number of SNARE complexes at the fusion pore using the t-SNARE recruitment model of ref. [1]

In the main text ("At high cholesterol levels fusion is so accelerated that there is insufficient time to recruit t-SNAREs to the fusion site," Fig. **5**A) we report the number of t-SNAREs recruited during the docking-to-fusion delay time by vesicle v-SNAREs using the SNARE recruitment model that we previously developed in ref. (1). This procedure provides an estimate of the number of SNAREpins involved in fusion for each membrane composition, reported in Fig. **5**A of the main text.

t-SNARE recruitment model. In ref. (1), we developed a t-SNARE recruitment model to determine the number of t-SNAREs, $N^{\star}$, recruited to the vesicle a time τ after the vesicle is docked by formation of the first SNARE complex. The key model assumptions were: (1) t-SNAREs are homogeneously and randomly distributed throughout the SBL with density Γ_{S} and diffuse independently with diffusivity D_{S}; (2) when a t-SNARE diffuses into the "reaction sink"

region of radius b beneath the vesicle, it immediately binds an available vesicle v-SNARE to form a SNAREpin; (3) fusion occurs instantly when p SNAREpins have formed. Thus solving the reaction-diffusion equation governing t-SNARE diffusion and binding with v-SNAREs, the model-predicted mean number of t-SNAREs recruited after time τ is

$$N^{\star}(\tau) = \frac{4\pi\Gamma_{\mathrm{S}} D_{\mathrm{S}} \tau}{\ln(c_1 \tau/\tau_{\mathrm{b}})}, \tau_{\mathrm{b}} = b^2/D_{\mathrm{S}}\,, \qquad \textbf{S13}$$

where the numerical constant $c_1 = 1.247$. Here we evaluate eq. **S13** at the measured mean delay time to fusion ($\tau = \overline{\tau}_{\mathrm{delay}}$). Thus after accounting for the initial SNAREpin which docks the vesicle, the total number of SNAREpins p participating in the fusion process for that vesicle is

$$p = \frac{4\pi\Gamma_{\mathrm{S}} D_{\mathrm{S}} \overline{\tau}_{\mathrm{delay}}}{\ln(c_1 \overline{\tau}_{\mathrm{delay}}/\tau_{\mathrm{b}})} + 1 \qquad \textbf{S14}$$

Below we estimate the values of the parameters in eq. **S14** and thus estimate the number of SNAREpins recruited for each membrane composition, $p - 1$.

Parameter values. To evaluate the t-SNARE diffusivity, we assumed the ratio $D_{\mathrm{s}}/D_{\mathrm{lip}}$ remained constant across different compositions and equal to 0.10, the value of this ratio that was used in ref. (1) based on the SNARE diffusivity measured by Wagner and Tamm (7). Using the single lipid diffusivity values of Table S**3** for all SBL compositions gives t-SNARE diffusivities of 0.17, 0.12, 0.15, and 0.04 μm^2/s. Assuming that the mobile, active fraction of t-SNAREs in the SBL is 0.5 (1, 7), the density of mobile t-SNAREs is $\Gamma_{\mathrm{S}} = 41.67/\mu m^2$ for our lipid to protein ratio (t-L:P=20,000). We take the sink size b=10 nm as in ref. (1).

Recruitment model predictions. Let us define $n = p - 1$ to be the number of t-SNAREs recruited to the fusion site before fusion occurs. Using the parameter estimates above in eq. **S14** predicts $n = 6 \pm 3$ and $n = 3 \pm 1$ for the model composition and the cholesterol free physiological composition PC/PS and PC/PS/PE/PIP2, respectively, and $n = 3 \pm 2$ for physiological compositions with 45% cholesterol in the SUV membranes and 10% cholesterol in the SBL membranes. (Note the reported uncertainties in n are lower-bounds estimated by propagating only the uncertainty in τ_{delay} values.) These n values are consistent with the range n ~ 3-10 reported in refs. (1, 8). In clear contrast, the same procedure when applied to physiological compositions with 46% cholesterol in both the SUV and SBL membranes

predicted that only $n = 0.15 \pm 0.02$ SNAREpins are recruited during the delay to fusion, suggesting that there is insignificant time for even a single additional t-SNARE to be recruited to the fusion site after docking.

As discussed in the main text, this could indicate that t-SNAREs are preclustered at docking sites with high densities.

Dependence of the TIRF fluorescence reduction factor $\boldsymbol{\lambda_{\mathrm{TIRF}}}$ on vesicle radius $\boldsymbol{R_{\mathrm{ves}}}$: coupled contributions from incident evanescent intensity decay and polarization effects

In Fig. **6D** of the main text we plotted values of $\boldsymbol{\lambda_{\mathrm{TIRF}}}$ versus $\boldsymbol{R_{\mathrm{ves}}}$ obtained from our analyses of many fusion events. Here, we discuss the theoretical relationship between these two quantities based on the known characteristics of TIRF microscopy. From this relation we determined the tangent of the relation at zero vesicle radius and we fit the tangent to the data of Fig. **6D.**

Consider a vesicle of radius R_{ves} docked at the SBL as in Fig. **6**A. The total TIRF fluorescence emission intensity of the vesicle is a sum over all lipid orientations θ in the spherical vesicle membrane

$$I_{\mathrm{dock}} = \epsilon I_{\mathrm{inc}}^{\mathrm{o}} \rho_{\mathrm{lip}} \mu_{\mathrm{Q}} \int_0^{\pi} d\theta 2\pi R_{\mathrm{ves}}^2 \sin\theta \, \alpha_{\mathrm{P}}(\theta) e^{-R_{\mathrm{ves}}[1+\cos\theta]/\delta_{\mathrm{TIRF}}} . \qquad \textbf{S15}$$

Here $I_{\mathrm{inc}}^{\mathrm{o}}$ is the incident TIRF intensity at the SBL ($z = 0$), ϵ is the single fluorescent lipid emissivity, δ_{TIRF} is the TIRF decay length and $\mu_{\mathrm{Q}} \leq 1$ is the fluorescence quenching factor due to a higher labeled lipid density in the vesicle. The mean polarization factor per lipid, $\alpha_{\mathrm{P}}(\theta)$, is the factor by which the lipid intensity is reduced (or enhanced) due to its orientation, for a segment of the vesicle bilayer with outward normal oriented at angle θ relative to the SBL normal. We define this factor relative to the situation when the lipid resides in the SBL ($\theta = 0$): hence $\alpha_{\mathrm{P}}(0) \equiv 1$. It arises because the evanescent TIRF wave is polarized, and preferentially excites fluorescent labels whose excitation dipoles align with its polarization (9). α_{P} is the mean value per lipid, and is a weighted average over all labeled lipids in the inner and outer monolayers of the local vesicle segment. In general it is expected to depend on bilayer curvature,

labeled and unlabeled lipid density and the partitioning of labeled lipids between the two monolayers.

Following fusion of the vesicle, the labeled lipids will be released into the SBL and after sufficient time will have diffused to be dilute enough for full dequenching to have occurred. The polarization factor for the lipids is then unity. Thus, the total intensity of the released lipids in the SBL is given by:

$$I_{\mathrm{dock}} = \epsilon I^{\mathrm{o}}_{\mathrm{inc}} \rho_{\mathrm{lip}} 4\pi R^2_{\mathrm{ves}} \qquad \textbf{S16}$$

The fluorescence reduction factor is the ratio of the total intensities before and after fusion:

$$\lambda_{\mathrm{TIRF}}(R_{\mathrm{ves}}) = \frac{I_{\mathrm{dock}}}{I_{\mathrm{SBL}}} = \frac{\mu_{\mathrm{Q}}}{2} \int_0^{\pi} d\theta \sin\theta \, \alpha_{\mathrm{P}}(\theta) e^{-R_{\mathrm{ves}}[1+\cos\theta]/\delta_{\mathrm{TIRF}}} \qquad \textbf{S17}$$

We are interested in the form of λ_{TIRF} as a function of R_{ves}. It is clear from the integral in eq. **S17** that this dependence is complex, as the effects of exponential TIRF intensity fall off and polarization are intimately coupled. Both effects are important. The only practical way to establish this crucial function, $\lambda_{\mathrm{TIRF}}(R_{\mathrm{ves}})$, is to directly measure it as described in the main text (Fig. **6**D).

Determining the pure polarization effect. Now taking the derivative of $\lambda_{\mathrm{TIRF}}(R_{\mathrm{ves}})$ with respect to R_{ves} and setting $R_{\mathrm{ves}} = 0$, one obtains a sum of two terms, $-\lambda_{\mathrm{TIRF}}(0)/\delta_{\mathrm{TIRF}} + \left(\mu_{\mathrm{Q}}/2\right) \int_0^{\pi} d\theta \sin\theta \cos\theta \, \alpha_{\mathrm{P}}(\theta)$. The second term vanishes, however, from the up-down symmetry of the polarization factor, $\alpha_{\mathrm{P}}(\theta) = \alpha_{\mathrm{P}}(\pi - \theta)$. Thus

$$\left(\frac{\partial \lambda_{\mathrm{TIRF}}}{\partial R_{\mathrm{ves}}}\right)_{R_{\mathrm{ves}}=0} = \frac{-\lambda_{\mathrm{TIRF}}(0)}{\delta_{\mathrm{TIRF}}}, \lambda_{\mathrm{TIRF}}(0) = \left(\frac{\mu_{\mathrm{Q}}}{2}\right) \int_0^{\pi} d\theta \sin\theta \, \alpha_{\mathrm{P}}(\theta) \, . \qquad \textbf{S18}$$

This shows that, at zero vesicle radius, λ_{TIRF} and its slope are determined by a simple moment of the polarization factor $\alpha_{\mathrm{P}}(\theta)$. To obtain $\lambda_{\mathrm{TIRF}}(0)$, in principle one could measure λ_{TIRF} versus vesicle radius (as described in this paper) and extrapolate to zero radius. In the main text we outlined an alternative procedure to obtain $\lambda^{\mathrm{o}}_{\mathrm{TIRF}} \equiv \lambda_{\mathrm{TIRF}}(0)$ which is based on the slope at the origin, and is preferable because our data is noisiest for small vesicles, whose small lipid release times are covered by fewest time frames in our intensity profiles. For small R_{ves} (we used data points with $R_{\mathrm{ves}} < 35$ nm) we fit our λ_{TIRF} versus R_{ves} data to a linear relation with the correct slope, as given by eq. **S18** (dashed red line, Fig. **6**D). Constraining this tangent to have intercept

$R_{\mathrm{ves}} = \delta_{\mathrm{TIRF}} = 68$ nm, the experimentally measured evanescent field penetration depth (see Materials and Methods), and extrapolating to zero vesicle size we could read off $\lambda^{\mathrm{o}}_{\mathrm{TIRF}} = 0.81 \pm 0.03$. For our experimental system, $\lambda^{\mathrm{o}}_{\mathrm{TIRF}}$ is essentially a pure polarization effect because self-quenching is expected to be negligible at the dilute lipid labeling densities we used (0.6-0.8 mole %, see Table S1).

Quantitative model of the effect of cholesterol on the fusion pore bending energy

A number of theoretical studies have analyzed the energetics of the membrane fusion pore (10, 11). Here we estimated the reduction by cholesterol of the bending energy of the highly bent fusion pore using a simple extension of a mathematical model developed in ref. (12). This is a strong effect because cholesterol has negative spontaneous curvature, and the fusion pore has a net negative curvature. The model quantifies the elastic properties of the lipid leaflets that constitute the pore. Our aim is to predict the influence of cholesterol on the free energy of pore formation, ΔF_{pore}, which is closely related to pore openness P_0 (see main text).

Consider two planar bilayers, whose neutral surfaces are separated by distance 2h (Fig. **S5**A). We assume each bilayer is symmetric and we will consider each of the physiologically motivated compositions that we treated in our experimental study (PC/PS/PE/PIP2, PC/PS/PE/PIP2/Ch, PC/PS/PE/PIP2/Ch+, Tables **S1, S2**.). What is the free energy to create a fusion pore, ΔF_{pore}? How is this free energy change affected by the addition of cholesterol? We assume the pore is torroidal in shape (10) with radius r_{p}. Hence each monolayer of the pore is also torroidal with dimensions adjusted by the monolayer thickness δ (Fig. **S5**A). Kozlov et al (12) calculated the elastic bending energy of such torroidal monolayers as

$$F_{\mathrm{monolayer}} = \pi\kappa \left\{ \frac{2\left(h + r_{\mathrm{p}}\right)^2}{h\sqrt{r_{\mathrm{p}}\left(r_{\mathrm{p}} + 2h\right)}} \operatorname{atan} \sqrt{\frac{r_{\mathrm{p}} + 2h}{r_{\mathrm{p}}}} + C_{\mathrm{o}}\left[2\pi\left(r_{\mathrm{p}} + h\right) - 8h\right] - 4 \right\} \qquad \textbf{S19}$$

where κ is the monolayer bending modulus and C_{o} is the monolayer spontaneous curvature. We applied this equation to the situation of two monolayers that constitute a fusion pore as follows. (1) Pore geometry required that the parameter h for membrane separation be increased

(decreased) by one-half of the monolayer thickness of 2 nm for the inner (outer) leaflets; we took an intermembrane headgroup separation of 7 nm so accordingly we used h=4.5 nm for the outer leaflets and h=6.5 nm for the inner leaflets. (2) Similarly the pore radius r_{p} was increased (decreased) by one-half of the monolayer thickness of 2 nm for the outer (inner) leaflets. (3) We calculated the spontaneous curvature C_{o} by taking the weighted average of all C_o values for the individual lipid species in the bilayer. For the inner and outer leaflets we used in the formula of Eq. S19 a spontaneous curvature equal to $-C_0$ and $+C_0$, respectively, reflecting the opposite orientations of the two leaflets. (4) We took the monolayer bending modulus to be $\kappa =$ 12 kT (13). (5) We summed the outer and inner monolayer energies to find the total energy of pore formation, $\Delta F_{\mathrm{pore}} = F^{\mathrm{outer}}_{\mathrm{monolayer}} + F^{\mathrm{inner}}_{\mathrm{monolayer}}$. For each membrane composition we allowed the pore radius to anneal, and we found that the pore radius corresponding to the lowest free energy of the fusion pore was independent of the spontaneous curvature of the individual leaflets.

To examine the mechanisms by which cholesterol may promote the open state of the fusion pore, we calculated the free energy advantage of adding cholesterol to the leaflets. In eq. **S19**, the different amounts of cholesterol had the effect of changing C_{o} (we assumed bending modulus κ was unaffected). To calculate the spontaneous curvature C_{o} for each level of cholesterol, we took the weighted average of the spontaneous curvature of each of the components. We took the spontaneous radius of curvatures of PC, PS, PE, and cholesterol to be -9.9, 14.4, -2.8, and -2.7 nm, respectively (13, 14). We find that the addition of moderate levels of cholesterol to physiological mimic compositions (45% and 10% cholesterol in SUV and SBL membranes, respectively, composition PC/PS/PE/PIP2/Ch) lowers the free energy of pore formation by ~8 kT, while with physiological cholesterol levels (46% in all membranes PC/PS/PE/PIP2/Ch+) the free energy of pore formation was lowered by ~43 kT (Fig. **S5**B). We note that the predicted free energies should be viewed as semi-quantitative because for simplicity of calculation it was assumed that the membranes are planar away from the pore, whereas in reality the vesicle membrane is curved.

Lipid compositions used in this study (details)

Symbol	PC (%)	DOPS (%)	SAPE (%)	PIP2 (%)	Chol (%)	Label (%)	PEG-PE	Label
$\boldsymbol{\alpha^{+}_{chol}}$	22.53	11.57	15.43	-	45.99	0.62	3.86	LR-PE
$\boldsymbol{\alpha_{chol}}$	23.75	12	15	-	45	0.8	3.45	LR-PE
	23.55	12	15	-	45	1	3.45	DiI
$\boldsymbol{\alpha}$	67.2	12	15	-	-	0.8	5	LR-PE
	67	12	15	-	-	1	5	DiI
	59.2	15	20	-	-	0.8	5	LR-PE
$\boldsymbol{\beta}$	79.2	15	-	-	-	0.8	5	LR-PE

Table S1-Lipid compositions for vesicle membranes. Symbols $\boldsymbol{\alpha^{+}_{chol}}$, $\boldsymbol{\alpha_{chol}}$, $\boldsymbol{\alpha}$, **and** $\boldsymbol{\beta}$ denote PC/PS/PE/PIP2/Ch+, PC/PS/PE/PIP2/Ch, PC/PS/PE/PIP2, and PC/PS, respectively. PC denotes 1-palmitoyl-2-oleoyl-*sn*-glycero-3-phosphocholine, POPC, except for composition $\boldsymbol{\beta}$ where it denotes 1,2-dioleoyl-*sn*-glycero-3-phosphocholine, DOPC; DOPS denotes 1,2-dioleoyl-*sn*-glycero-3-phospho-L-serine; SAPE denotes 1-stearoyl-2-arachidonoyl-*sn*-glycero-3-phosphoethanolamine; PIP2 denotes phosphatidylinositol 4,5-bisphosphate; LR denotes the fluorescent group lissamine rhodamine B.

Symbol	PC (%)	DOPS (%)	SAPE (%)	PIP2 (%)	Chol (%)	Label (%)	PEG-PE (%)
$\boldsymbol{\alpha^{+}_{chol}}$	18.91	11.57	15.43	3.86	45.99	0.38	3.86
$\boldsymbol{\alpha_{chol}}$	54.9	12	15	3	10	0.5	4.6
$\boldsymbol{\alpha}$	64.5	12	15	3	-	0.5	5
	54.5	15	20	5	-	0.5	5
$\boldsymbol{\beta}$	79.5	15	-	-	-	0.5	5

Table S2- Lipid compositions for SBL membranes. Symbols have same meaning as for Table S1. Label for SBL is NBD-PE, which denotes 1,2-dioleoyl-sn-glycero-3-phosphoethanolamine-N-(7-nitro-2-1,3-benzoxadiazol-4-yl).

Symbol	D_{lip} $(\mu m^2/s)$	Label
α^{+}_{chol}	0.45	LR-PE
α	1.17	LR-PE
	1.43	DiI
α_{chol}	1.49	LR-PE
	2.39	DiI
β	1.7	LR-PE

Table S3- Diffusion constants for each lipid membrane composition studied, and for each label used. Calculated from the measured mean square displacement curves for each composition (Fig. **S2B**).

Supporting References Cited

1. Karatekin, E., J. Di Giovanni, C. Iborra, J. Coleman, B. O'Shaughnessy, M. Seagar, and J. E. Rothman. 2010. A fast, single-vesicle fusion assay mimics physiological SNARE requirements. Proceedings of the National Academy of Sciences 107:3517-3521.
2. Smith, M. B., E. Karatekin, A. Gohlke, H. Mizuno, N. Watanabe, and D. Vavylonis. 2011. Interactive, Computer-Assisted Tracking of Speckle Trajectories in Fluorescence Microscopy: Application to Actin Polymerization and Membrane Fusion. Biophysical journal 101:1794-1804.
3. Klyachko, V. A., and M. B. Jackson. 2002. Capacitance steps and fusion pores of small and large-dense-core vesicles in nerve terminals. Nature 418:89-92.
4. Breckenridge, L., and W. Almers. 1987. Final steps in exocytosis observed in a cell with giant secretory granules. Proceedings of the National Academy of Sciences 84:1945.
5. Monck, J. R., and J. M. Fernandez. 1992. The exocytotic fusion pore. The Journal of Cell Biology 119:1395.
6. He, L., X. S. Wu, R. Mohan, and L. G. Wu. 2006. Two modes of fusion pore opening revealed by cell-attached recordings at a synapse. Nature 444:102-105.
7. Wagner, M. L., and L. K. Tamm. 2001. Reconstituted syntaxin1a/SNAP25 interacts with negatively charged lipids as measured by lateral diffusion in planar supported bilayers. Biophysical journal 81:266-275.
8. Shi, L., Q. T. Shen, A. Kiel, J. Wang, H. W. Wang, T. J. Melia, J. E. Rothman, and F. Pincet. 2012. SNARE proteins: one to fuse and three to keep the nascent fusion pore open. Science Signalling 335:1355.
9. Axelrod, D. 1989. Total internal reflection fluorescence microscopy. Method Cell Biol. 30:245-270.
10. Chizmadzhev, Y. A., F. Cohen, A. Shcherbakov, and J. Zimmerberg. 1995. Membrane mechanics can account for fusion pore dilation in stages. Biophysical journal 69:2489-2500.
11. Jackson, M. B. 2009. Minimum membrane bending energies of fusion pores. J. Membr. Biol. 231:101-115.
12. Kozlov, M. M., S. L. Leikin, L. V. Chernomordik, V. S. Markin, and Y. A. Chizmadzhev. 1989. Stalk mechanism of vesicle fusion - intermixing of aqueous contents. Eur. Biophys. J. Biophys. Lett. 17:121-129.
13. Chen, Z., and R. Rand. 1997. The influence of cholesterol on phospholipid membrane curvature and bending elasticity. Biophysical journal 73:267-276.
14. Fuller, N., C. R. Benatti, and R. Peter Rand. 2003. Curvature and bending constants for phosphatidylserine-containing membranes. Biophys. J. 85:1667-1674.

Supplementary Figures

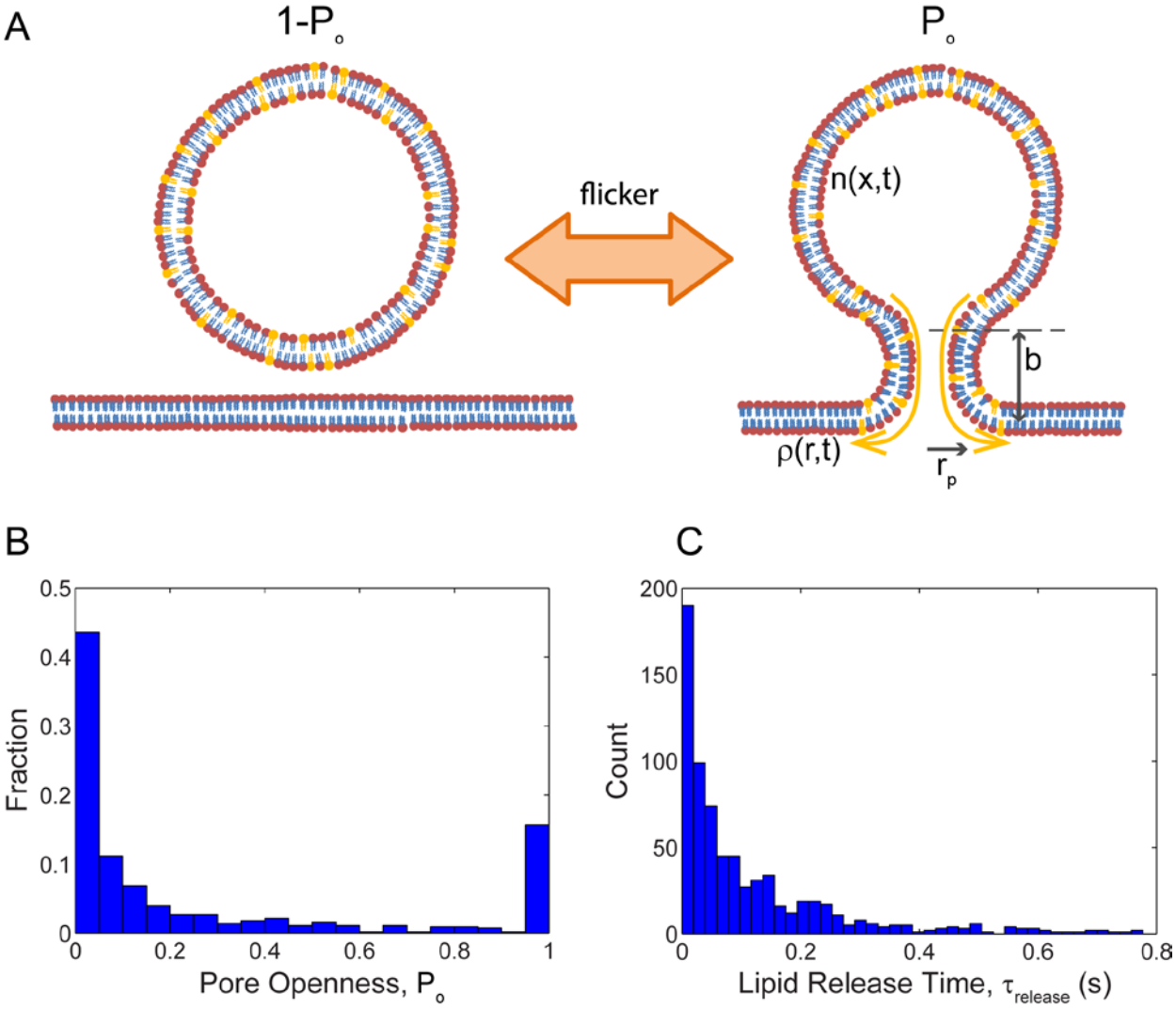

Figure S1- (A) Model of lipid release from a vesicle through a flickering fusion pore. Schematic of model. The pore is centered at $x = 0$ in the vesicle and $r = 0$ in the SBL. The density of labelled lipids in the vesicle is $n(x,t)$ and in the SBL is $\rho(r,t)$. Here, we model the pore as a cylinder of length $b = 15$ nm and radius $r_p = 3$ nm. The pore radius is measured from the center of the pore to the centerline of the bilayer. During open periods of the pore, lipids can diffuse through the membranes of the neck of the pore into the SBL membranes; the net flux is proportional to the density difference across the pore multiplied by the fraction of the time the pore is open, P_o (eqs. S1 and S2). (B) Measured overall distribution of P_o values, for all compositions. Mean openness for flickering pores is 0.14 ± 0.01 and the fraction of pores that are permanently open is 15%. Bin size 0.05. (C) Measured distribution of lipid release times across all compositions. Bin size is 0.02 s.

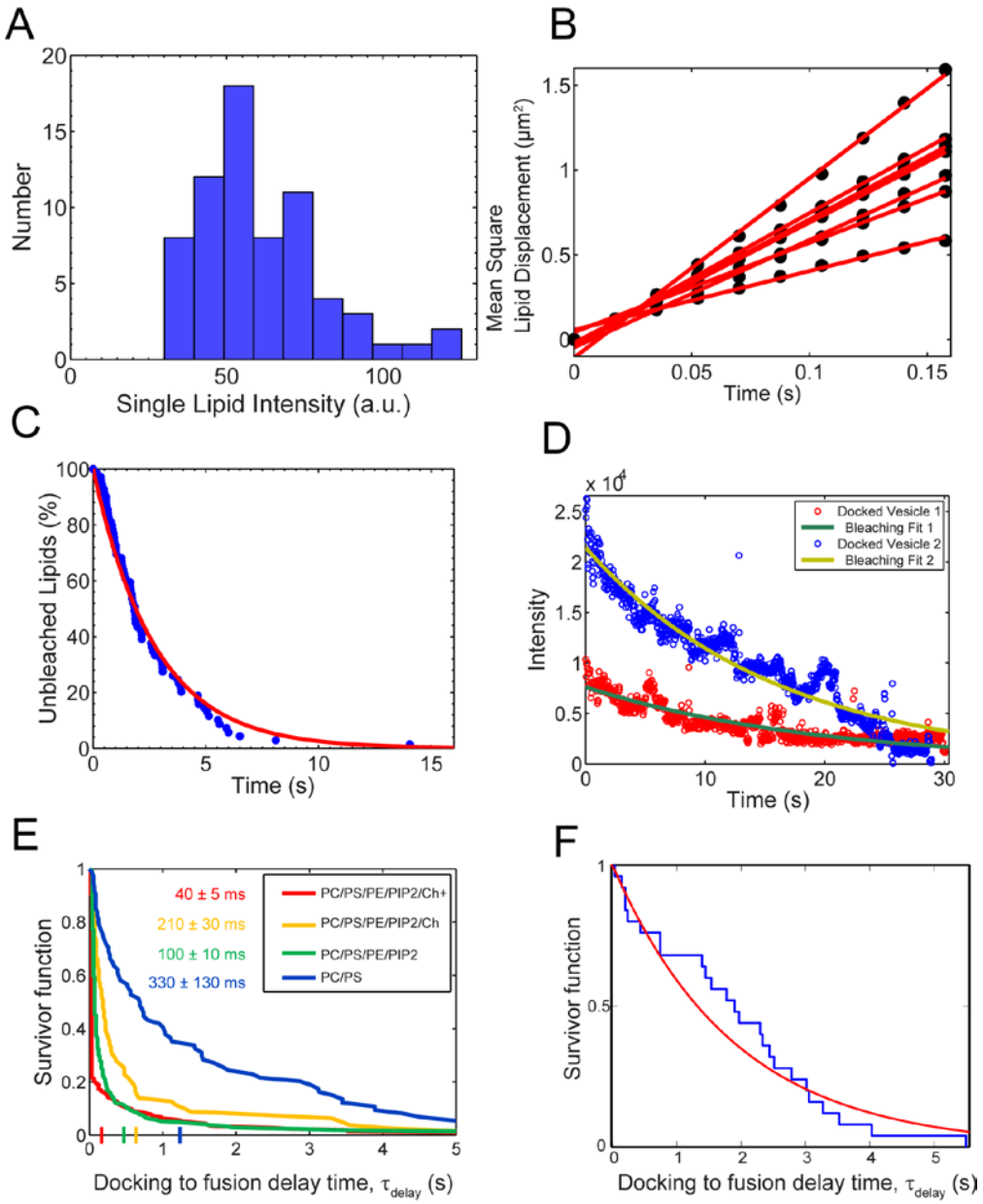

Figure S2- Single lipid properties needed for fusion event analysis, and measured docking-to-fusion delay time distributions. (A-C) Single lipid resolution enables accurate measurement of diffusivity, bleaching time and single lipid emission. Plots shown for PC/PS membrane composition. (A) Distribution of measured single lipid intensities, I_{lip}, in a typical movie. (B) Mean square displacement versus time for seven lipid trajectories. (C) Digital measurement of bleaching time τ_{bleach}. Labeled lipids in the SBL suddenly ceased fluorescing, indicating that these fluorescing spots were individual lipids. The survivor fraction is shown for a sample movie, fit to an exponential $\exp -t/\tau_{\mathrm{bleach}}$ (red curve). (D) Bleaching of lipids in vesicles is much slower than for lipids in the SBL. Emission intensity versus time for two representative unfused vesicles. Each is shown with a best fit curve to a decaying exponential $I(t) = e^{-t/\tau_{\mathrm{bleach}}^{\mathrm{ves}}}$ where $\tau_{\mathrm{bleach}}^{\mathrm{ves}}$ is the bleaching time in the vesicle. Both events are for PC/PS/PE/PIP2/Ch+ membrane composition. The bleaching time of the Docked Vesicle 1 (data: red points, best fit exponential:

green curve) is 19.9 s. The bleaching time for Docked Vesicle 2 (data: blue points, best fit exponential: gold curve) is 16.0 s. Both values are much greater than $3s \lesssim \tau_{\mathrm{bleach}} \lesssim 5s$, the bleaching time in the SBL. (E) Docking-to-fusion delay time distributions: measured survivor functions for all compositions. Mean delay times $\overline{\tau}_{\mathrm{delay}}$ for each composition are shown, along with 95% confidence interval. Colored ticks on the x-axis indicate the cutoff times used to separate the SNARE-mediated and non-specific fusion events. The cutoff times were obtained by fitting double exponentials to the survivor functions. (F) Docking-to-fusion delay time distributions for fusions between protein-free SBLs and v-SNARE containing SUVs, for lipid composition PC/PS/PE/PIP2/Ch that contains 45% (10%) cholesterol in the SUV (SBL) (see Tables **S1, S2**). Measured survivor function (blue curve) and best fit exponential (red curve) with delay time $\overline{\tau}_{\mathrm{pf}} = 1.9$ s are plotted. There is no statistically significant difference between this distribution and the long tail of the slow component of the delay time distribution for PC/PS/PE/PIP2/Ch fusion events between v-SUVs and t-SBLs ($p>0.05$), part (E).

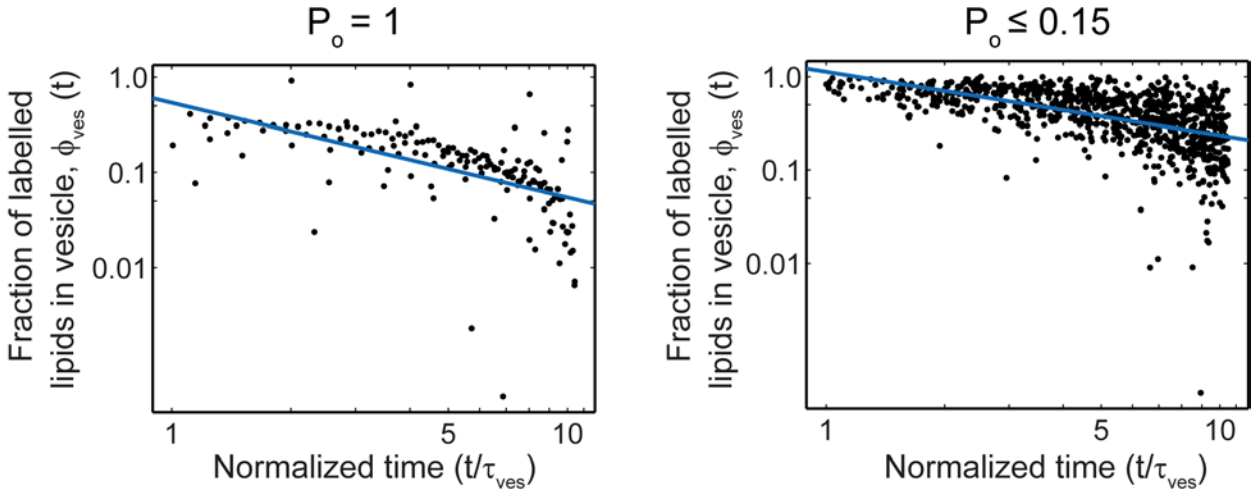

Figure S3- Vesicle-to-SBL lipid release kinetics through permanently open pores have power law dependence on time. Our model predicts that the number of lipids remaining in the vesicle decays as $\phi_{\mathrm{ves}}(\mathrm{t}) \sim \tau_{\mathrm{ves}}/t$ for a fully open fusion pore where τ_{ves} is the diffusion time on the scale of the vesicle and depends on vesicle size (see main text). The pooled $\phi_{\mathrm{ves}}(t)$ data that we measured for all fully open fusion pores ($P_{\mathrm{o}} = 1$, left panel) collapsed onto a single power law relation when plotted against time scaled with τ_{ves}. The best fit power law (blue line) was $t^{-\alpha}$ with $\alpha = -0.99 \pm 0.22$, very close to the model prediction. The same procedure applied to flickering pores with relatively small openness ($P_{\mathrm{o}} \leq 0.15$, right panel) produced a best fit power law exponent $\alpha = -0.68 \pm 0.09$.

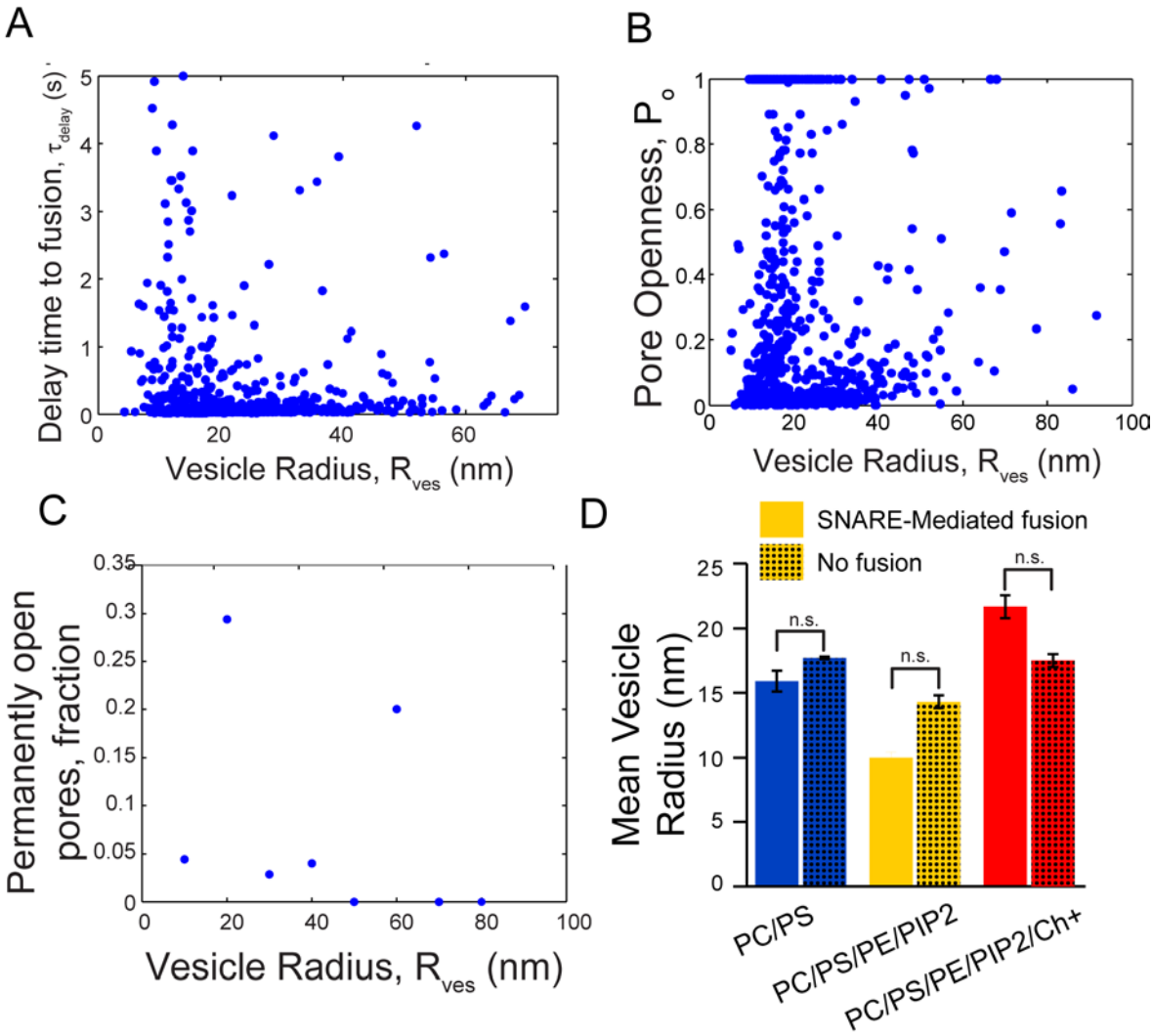

Figure S4- Statistics of fusion reveal no dependence on vesicle size. (A) Docking-to-fusion delay times versus vesicle size showed no correlations ($c_{\mathrm{corr}} = -0.04$, n=772, SNARE-mediated and non-specific events). Data shown represents all fusion events measured in this study for which both SBL and SUV membranes contained SNARES, for all compositions (Tables **S1,S2**). (B) Pore openness is not correlated with vesicle size, ($c_{\mathrm{corr}} = 0.05$, n=555 specific fusion events). Data shown represents all SNARE-mediated fusion events measured in this study (fast component of delay time distribution) for all compositions. (C) Fraction of pores that are permanently open is not correlated with vesicle size (c_{corr} = -0.04). Bin size 10nm. Same fusion events as for (B). (D) Mean size of vesicles that undergo SNARE-mediated fusion (solid bars) is statistically indistinguishable from mean size of docked vesicles that do not fuse during the bleaching time (dotted bars), $P > 0.05$. The comparison is shown for three lipid membrane compositions.

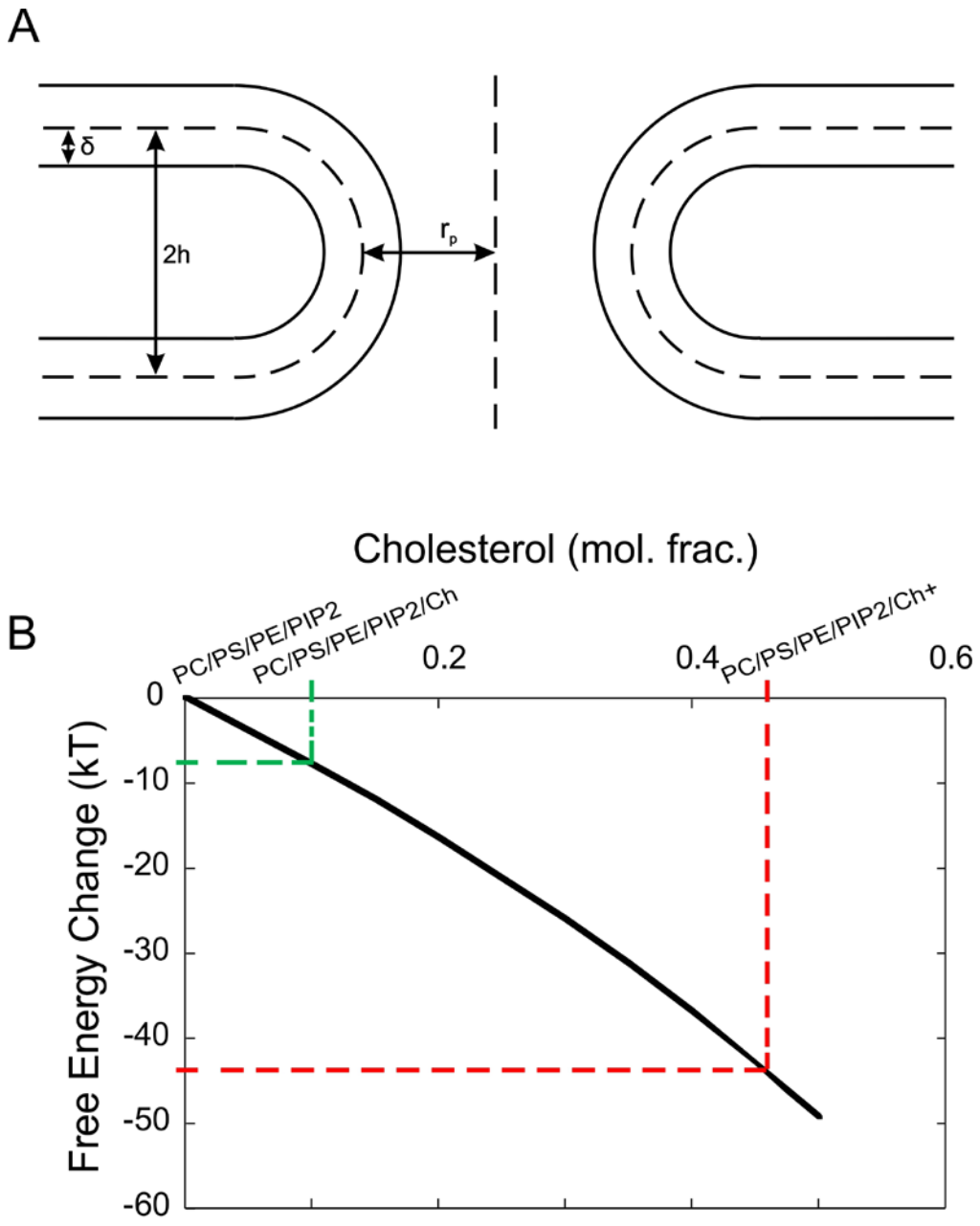

Figure S5- Cholesterol lowers the bending energy of fusion pores: calculation of pore bending energy using an elastic model of the fusion pore. (A) Schematic of a fusion pore, side view. The membranes have asymptotic separation 2h and the pore radius is r_p. Each leaflet has thickness δ. (B) Free energies were calculated for the biologically motivated family of lipid compositions (Tables S1, S2) using eq. **S20**. The change in free energy of pore formation relative to zero cholesterol (PC/PS/PE/PIP2) is plotted versus cholesterol content. Values for the two cholesterol-rich compositions studied (PC/PS/PE/PIP2/Ch, PC/PS/PE/PIP2/Ch+) are indicated. High cholesterol levels produce enormous free energy decreases, indicating a powerful stabilizing effect on the open state of the pore.

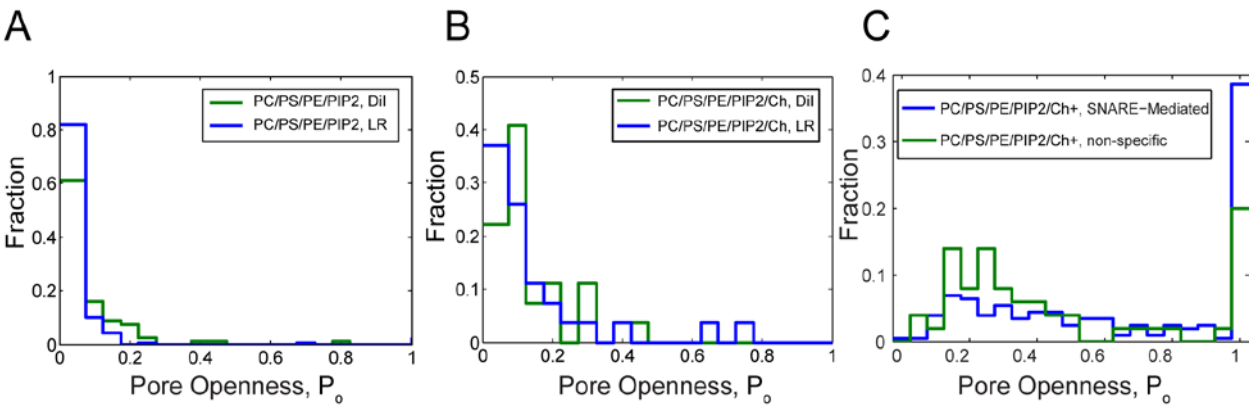

Figure S6- (A, B). Measured distributions of pore openness were not significantly different ($p>0.05$, student's t-test) for two distinct fluorescent lipid labels, lissamine-rhodamine-tagged PE (LR-PE) and the lipophilic dye DiI. This was true for both lipid compositions PC/PS/PE/PIP2 and PC/PS/PE/PIP2/Ch. These results are consistent with LR-PE diffusion not being anomalously suppressed in the fusion pore and the validity of the P_o values inferred from release kinetics of LR-PE through fusion pores. (C) Distributions of fusion pore openness for SNARE-mediated and non-specific fusion events between membranes having high cholesterol content (lipid composition PC/PS/PE/PIP2/Ch+). The fraction of pores that were fully open was ~2-fold higher when SNAREs mediated the pores.

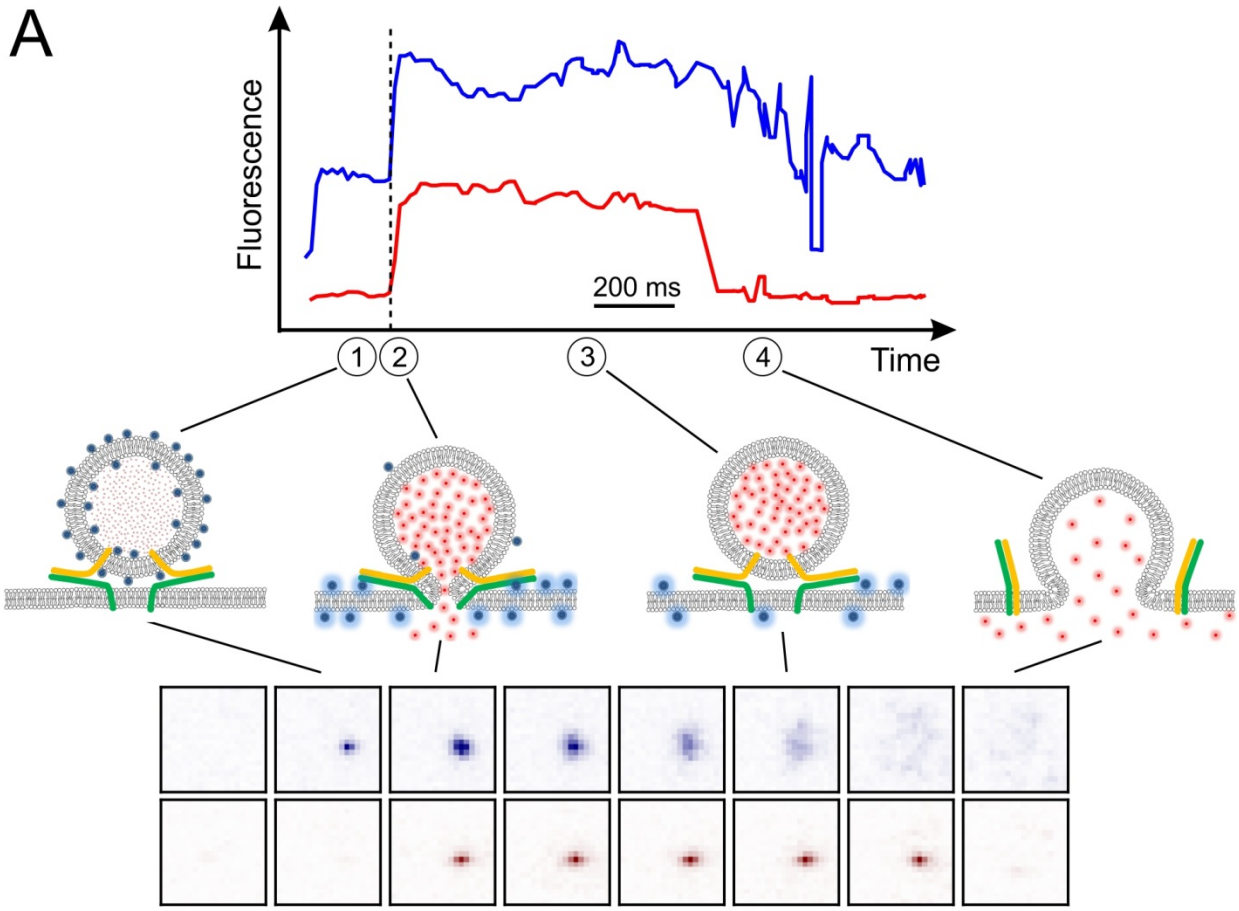
A
Fluorescence
200 ms
Time
1
2
3
4

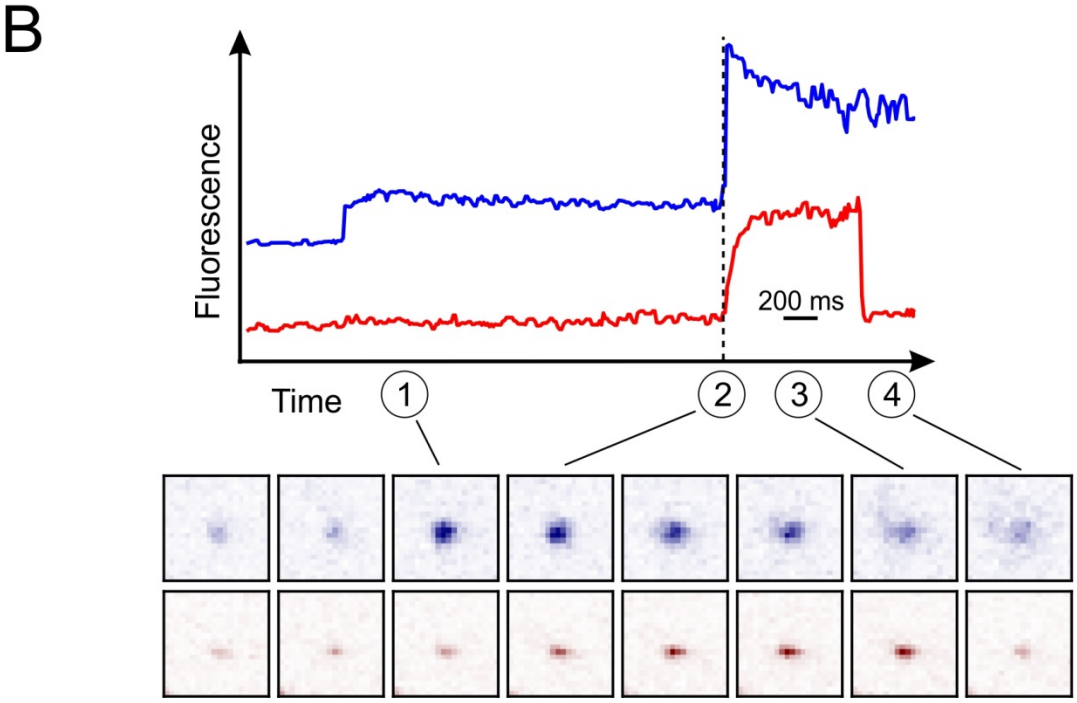
B
Fluorescence
200 ms
Time
1
2
3
4

Figure S7- Additional examples of simultaneous contents and lipid release during v-SUV/t-SBL fusion, measured with TIRFM (cf. Fig 3). (A) vSUVs with 45 mole % cholesterol, (B) cholesterol-free vSUVs contained 1 mole % DiD lipid dye and encapsulated 10 mM soluble contents marker SRB. DiD and SRB were simultaneously excited using 638 nm and 561 nm laser lines, respectively. The emission was split to observe DiD (top trace, blue) and SRB (red trace) fluorescence signals simultaneously projected onto an EMCCD detector. Total intensities from a region 20 pixels by 20 pixels (5.3 μm x 5.3 μm) are plotted (18.3 ms resolution) for both the lipid (upper trace, blue) and contents (lower trace, red) signals for representative events. Snapshots from the lipid (blue) and contents (red) signals are shown in inverted false colors. When docking was clearly visible in the lipid channel, the contents channel was still dim, because SRB was encapsulated at self-quenching concentrations (#1). In the same frame in which the lipid signals begin to increase, announcing lipid mixing, the contents signals also increase (dashed vertical line), due to dilution and dequenching of encapsulated SRB as molecules escape through the pore. Once lipid transfer is complete (shortly after the maximum in the blue trace), the intensity in the lipid channel decreases due to photobleaching (#3), as in Fig. 2. The SRB signal was abruptly lost seconds after the initial dequenching (#4) in ~20% of events. .